

Design and Characterisation of a Metastable Helium Source

A thesis submitted for the degree of Master of Science

Nikolaus Traitler

University of York
Department of Physics
November 2002

Abstract

This thesis describes the design and characterisation of an apparatus to produce a beam of metastable helium atoms in the 2^3S state. The source is based on a cold-cathode DC electrical discharge. The design of the source is such that different parameters can be tested and the effect of them on the beam quality investigated. This inbuilt versatility is greater than in the work of others in this field.

A review of different types of metastable helium sources is provided. The purpose of the present source is for the study of surface properties using metastable de-excitation spectroscopy. This will involve laser cooling of the beam, which requires a slow beam with narrow velocity distribution. Other applications which are also described include neutral atom lithography and the study of Bose-Einstein Condensation.

The most important parameters in the geometry of the source and the way it is operated are identified. These include factors that were simple to change, such as the driving pressure in the source and the discharge voltage, but also factors that were more complex to change, such as the cathode-nozzle distance, the size of the nozzle orifice or the size of the tube in which the discharge is constraint.

The expansion of the helium from the source through the vacuum system has an important effect on the beam and is analysed in some detail. One of the most important influences on the number of metastable atoms is the partial pressure of impurities in the low pressure region in which the expansion occurs. The quality of the beam is described in terms of its intensity (flux), longitudinal velocity and velocity distribution. Methods of measuring these quantities are described.

Based on the optimal parameters obtained in this work and also incorporating some new ideas, suggestions for a new design are given, which will have the highest possible flux, and low velocity.

Contents

ABSTRACT	2
CONTENTS.....	3
LIST OF FIGURES	5
LIST OF TABLES	7
ACKNOWLEDGEMENTS.....	8
DECLARATION.....	9
1. INTRODUCTION.....	10
2. REVIEW OF PREVIOUS WORK.....	13
2.1. TYPES OF SOURCES.....	13
2.1.1. DC Discharges.....	14
2.1.2. Electron Impact Sources.....	16
2.1.3. Pulsed Discharges.....	17
2.2. APPLICATIONS OF METASTABLE ATOMIC BEAMS.....	17
2.2.1. Metastable De-excitation Spectroscopy	18
2.2.2. Surface Magnetic Properties.....	21
2.2.3. Microscopy	21
2.2.4. Neutral Atom Lithography	21
2.2.5. Bose-Einstein Condensates	23
2.3. SUMMARY	24
3. LASER COOLING AND THE EXPANDING BEAM.....	25
3.1. LASER COOLING	25
3.2. JET THEORY.....	28
3.2.1. Effusive Beams.....	28
3.2.2. Supersonic Expansions.....	28
3.2.3. The Mach Number.....	30
3.3. SUMMARY	32

4. EXPERIMENTAL SETUP	33
4.1. VACUUM SYSTEM.....	33
4.1.1. Vacuum Chamber Arrangement.....	33
4.1.2. Differential Pumping and Pumping Speeds	34
4.2. SOURCE DESIGN	38
4.2.1. Design Enabling Changes of Operating Parameters	38
4.3. OPERATION OF THE SOURCE	41
4.3.1. Electrical Circuitry	41
4.4. MEASUREMENT OF THE PROPERTIES OF THE BEAM	42
4.4.1. Removal of Unwanted Components from the Beam.....	42
4.4.2. Electron Emission Method	42
4.4.3. Time of Flight Technique	45
4.5. SUMMARY	47
5. RESULTS AND DISCUSSION	48
5.1. BEAM FLUX.....	50
5.1.1. Influence of Discharge Current on He* Yield	50
5.1.2. Influence of Driving Pressure on He* Yield.....	52
5.1.3. Attenuation of the Beam by Impurities	55
5.1.4. Influence of Source Geometry on He* Yield.....	56
5.2. VELOCITY DISTRIBUTION	58
5.2.1. Longitudinal Velocity.....	58
5.2.2. Velocity Width	60
5.3. OPTIMAL OPERATING PARAMETERS.....	62
5.3.1. Source Design Leading to Highest Yield	62
5.3.2. Discharge Current.....	63
5.3.3. Driving Pressure	63
5.4. SUMMARY	63
6. CONCLUSIONS AND FUTURE WORK.....	65
APPENDIX	67
REFERENCES.....	73

List of Figures

Figure 1 <i>Energy level diagram for helium</i>	11
Figure 2 <i>Schematic diagram of a typical DC discharge source</i>	15
Figure 3 <i>Schematic diagram of an electron bombardment source as used by Halfmann et al. [18]</i>	16
Figure 4 <i>Electron emission processes</i>	19
Figure 5 <i>The patterning process</i>	22
Figure 6 <i>Momentum transfer in spontaneous emission</i>	26
Figure 7 <i>Velocity distributions for different Mach numbers for He at 300K</i>	31
Figure 8 <i>Vacuum chamber arrangements</i>	34
Figure 9 <i>Pressures in the system</i>	36
Figure 10 <i>Schematic diagram of the source used in this work</i>	38
Figure 11 <i>Cross sectional view of the He* source used in this work</i>	40
Figure 12 <i>Schematic diagram of the electric circuitry of the source</i>	41
Figure 13 <i>Metastable detector</i>	43
Figure 14 <i>Dimensions of the system</i>	44
Figure 15 <i>Schematic diagram of the TOF technique</i>	46
Figure 16 <i>Typical time of flight spectrum</i>	48
Figure 17 <i>Velocity distribution</i>	49
Figure 18 <i>Measured intensity as a function of the discharge current</i>	51
Figure 19 <i>Current on the plate as a function of discharge voltage</i>	52
Figure 20 <i>Intensity of He* beam as a function of driving pressure using the electron emission method</i>	53
Figure 21 <i>He* flux as a function of driving pressure with pressure in the source chamber held constant</i>	54
Figure 22 <i>Residual gas spectrum from the source chamber</i>	55
Figure 23 <i>He* as a function of cathode-nozzle distance</i>	57
Figure 24 <i>Average flow velocity of He* atoms as a function of discharge current</i>	59
Figure 25 <i>Average flow velocity vs pressure in the source chamber</i>	60
Figure 26 <i>Velocity width as a function of discharge current</i>	61

Figure 27 <i>FWHM of the velocity distribution of the He* beam as a function of driving pressure</i>	62
Figure 28 <i>MCS-32 software for the TOF measurements</i>	68
Figure 29 <i>Smoothed spectrum compared to original spectrum</i>	72

List of Tables

Table 1 <i>Lifetime and energies of some transitions in helium</i>	12
Table 2 <i>Overview of metastable sources</i>	13

Acknowledgements

I would like to thank many people for the help they provided throughout the year. I would especially like to thank my supervisor Dr. Marcus Jacka for his advice and guidance throughout the project. His valuable help was also given in proof reading this thesis.

I would also like to thank the other members of our research group, especially Andy Kale, Andy Pratt and Mark Tyndall for their support and for making the lab a pleasant environment to work in.

I am also grateful to the technicians in the department, especially Dave Coulthard and Richard Armitage for leak testing the vacuum system and for their help with putting the vacuum system together. I must also thank Pete Durkin from the workshop who helped me with building the source.

Declaration

I declare that the work presented in this thesis is my own work and that contributions from others are acknowledged explicitly in the text or by means of references. This work has not been submitted previously for any other award or qualification.

Chapter 1

Introduction

Metastable excited helium states have a long lifetime since the transition to lower state levels is forbidden by dipole selection rules. For this reason and because of their large internal energy, metastable atoms are of fundamental interest in the field of surface and plasma physics [1, 2]. A summary of the relevant properties of the atoms is given in Table 1. There are many different ways to create metastable helium beams. In this work a cold cathode DC discharge source is used because it has a simple design and is stable for long periods of operation, which is desired for the work in our research group. The first metastable rare gas atomic beams using a DC discharge source were produced by Rothe *et al.* in 1965 [3]. The development of this and other types of sources is outlined in section 2.1.

The aim of this work is to produce an intense beam of metastable helium (He^*) atoms in the 2^3S_1 state and to investigate the effect of changing different parameters in the source design so as to optimise the flux. The beam will then be collimated using laser cooling techniques in future experiments. The resulting intense beam will be used primarily in surface spectroscopy. For laser cooling to be efficient, the metastable atomic beam should have a high flux, a low longitudinal velocity as well as a narrow velocity distribution. These properties can be measured using the time of flight (TOF) technique, which also gives the relative proportion of photons to the metastable components in the beam. A second technique, the electron emission method, allows further quantitative investigation of the intensity of the beam.

One application of the source in our work will be for the measurement of the magnetic properties of a surface. This will require the metastable atoms to be spin polarised. The transition used to spin polarise the atoms is the same as that used in the laser cooling of

the beam. Another potential application would be the use of the metastable beam in microscopy. Atom optic techniques, developed for lithography experiments, will be used to create a microscope with an array of probes each with a size of a few tens of nanometres in size. This will vastly improve the resolution and allow for much shorter acquisition times when compared to current microscopy techniques using metastable helium atoms.

The metastable 2^3S_1 state in helium is a very long lived state with a lifetime of 8000 seconds [4, 5]. The transition from the 1^1S_0 state to the 2^3S_1 state is dipole forbidden, but can occur by electron collisions in a discharge. The 2^3S_1 state also has a very high internal energy which makes He^* easily detectable. This high internal energy is the reason why it is of interest for many applications (see Section 2.2).

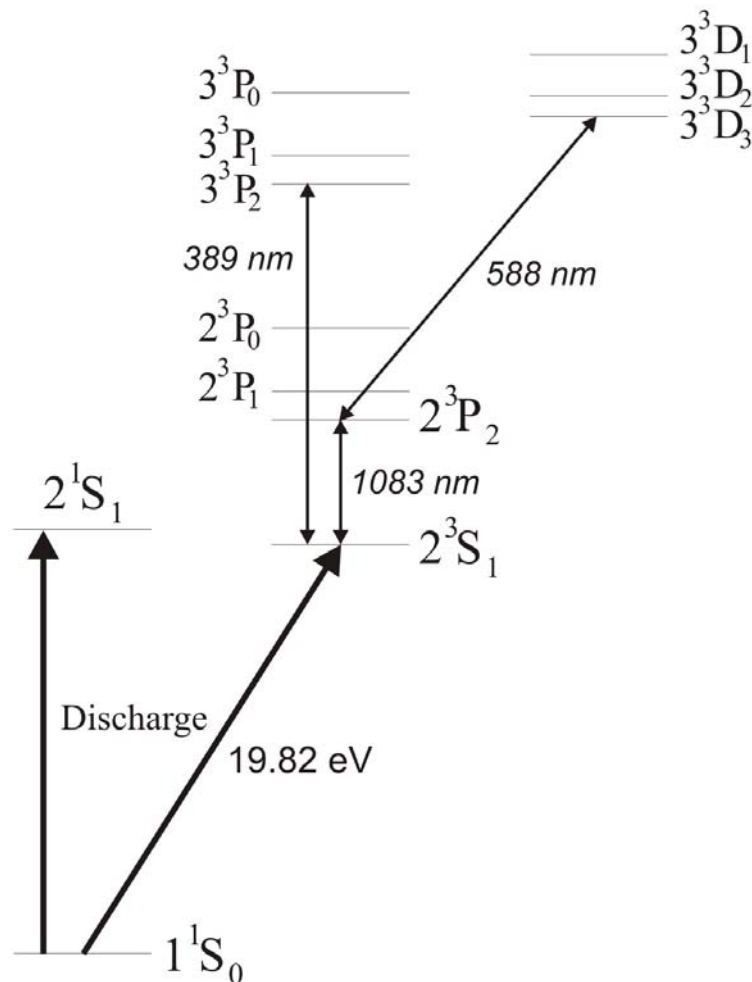


Figure 1 Energy level diagram for helium

Transition	$2^1S_0 - 2^3S_1$	$2^3S_1 - 2^3P_2$	$2^3S_1 - 3^3P_2$	$2^3P_2 - 3^3D_3$
Energy (eV)	19.82	1.144	3.192	2.109
Lifetime	8000 s	98.8 ns	95 ns	14 ns

Table 1 *Lifetime and energies of some transitions in helium*

The 2^1S state is also metastable, although with a much shorter lifetime. Both 2^1S and 2^3S are produced in a discharge source but the 2^1S state is not a good candidate for laser cooling because higher excited singlet states decay preferentially to ground rather than back to the 2^1S state.

Chapter 2

Review of Previous Work

2.1. Types of Sources

There are various techniques used to create beams of metastable atoms. The most commonly used sources are DC discharge sources [6,7], electron impact sources [8,9] and pulsed discharge sources [10,11]. In this work we will use a supersonic DC discharge source since it is simple to build and has a narrow velocity distribution compared to other types of sources. In these sources metastable atoms are created by excitation of ground state atoms by electron impact. In DC discharge sources the excitation occurs in the plasma region, whereas in electron impact sources an electron beam excites ground state atoms or molecules from effusive or supersonic beams.

A brief description of other types of sources will be given to put the current work in context. This will focus on those sources which produce a beam of metastable atoms rather than sources of metastables which are confined within a volume. The following table gives an overview of the different types of metastable sources discussed here.

Type of source	Flux ($\text{He}^* \text{ s}^{-1} \text{ sr}^{-1}$)	Comments	Reference
DC discharge	$3 \cdot 10^{12} - 2 \cdot 10^{15}$	High intensity, narrow velocity distribution	6, 7, 12, 13, 14
Electron bombardment	$2 \cdot 10^{10} - 4 \cdot 10^{14}$	Broad velocity distribution	9, 15, 16, 17
Pulsed discharge	$1.7 \cdot 10^{15} - 4 \cdot 10^{15}$	Not a continuous beam, complex design	10, 18

Table 2 *Overview of metastable sources*

Although pulsed discharges provide the highest He* flux, they are not well suited for our work since they do not provide a continuous flux of He* atoms. Electron bombardment sources have the disadvantage of having a broad velocity distribution due to momentum transfer from the electrons.

2.1.1. DC Discharges

There are many types of discharge sources such as hot-cathode effusive sources [3], effusive hollow-cathode arc sources [19] and supersonic cold cathode discharge sources [16]. In this work a supersonic cold cathode DC discharge source will be used to produce a metastable helium beam since this type of source is simple to build and the discharge is stable for a long period of operation. Supersonic DC discharge sources are the most commonly used types of sources. One problem of discharge sources is the relatively low fraction of metastable atoms in the beam. The ratio of metastables to ground state atoms in the beam is generally less than 10^{-4} . Discharge sources are generally simpler to construct than electron impact sources, however their velocity distribution is more difficult to control. The lifetime of such a source is mainly limited by the wear of the nozzle. The original design of this type of sources is by Searcy *et al.* [20] and the critical elements of such a source are shown in Figure 2. Supersonic discharge sources have a narrower velocity distribution than effusive ones, the reason for which will be explained later in section 3.2.2.

Most of the early designs are based on a discharge between a cold cathode rod and the skimmer across a nozzle approximately 0.15 mm in diameter. Another early design was proposed in 1975 by Leasure *et al.* [21] who used a high-voltage corona discharge between a sharp needle cathode and a cone-shaped anode. This source design produced a beam intensity of up to 10^{14} metastable helium atoms $\text{s}^{-1} \text{sr}^{-1}$. Fahey *et al.* [6] slightly improved this design by simplifying it and enhancing the beam flux.

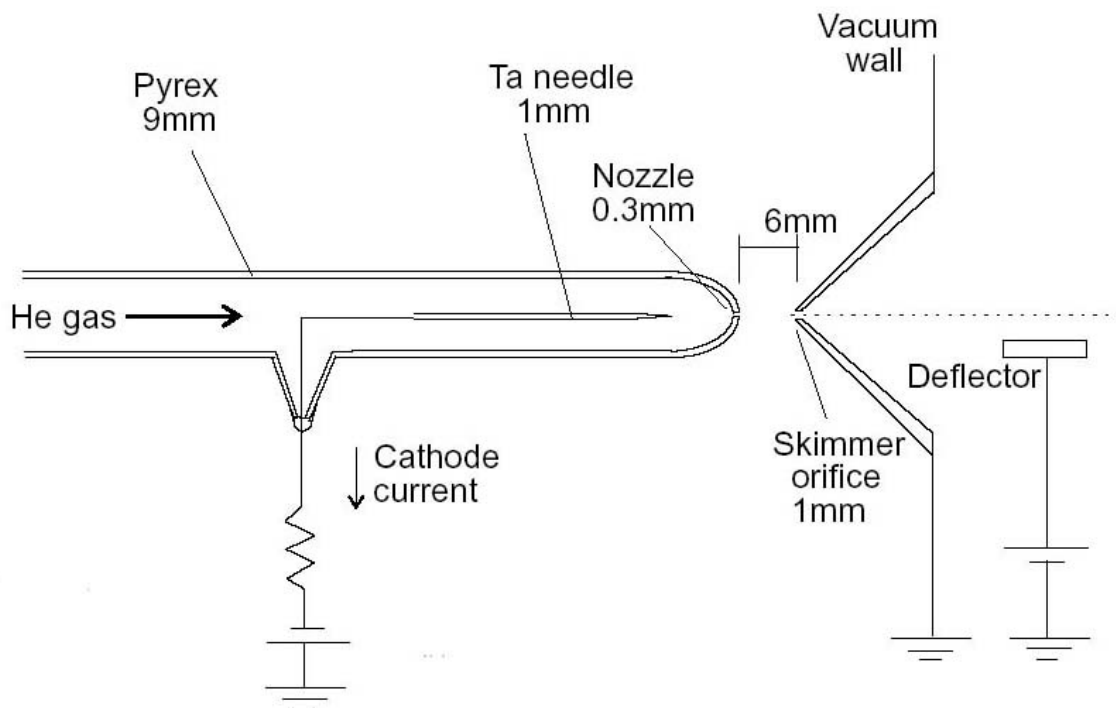


Figure 2 Schematic diagram of a typical DC discharge source

The discharge occurs between the needle and the skimmer. A deflector is used to remove the He ions from the beam.

A liquid nitrogen cooled DC discharge with a 0.25 mm nozzle diameter has been used by Rooijackers *et al.* [13] to produce an atomic beam of metastable helium atoms with an intensity of $2 \cdot 10^{14}$ metastable atoms $\text{s}^{-1} \text{sr}^{-1}$ and an average velocity of 1030 m/s. The discharge was maintained between a tantalum needle and the skimmer. The discharge current was varied between 2 and 13 mA and measured an intensity of $1.7 \cdot 10^{14}$ atoms $\text{s}^{-1} \text{sr}^{-1}$ and a velocity of 1030 m/s were measured at 2 mA. At 13 mA they found an intensity of $4.6 \cdot 10^{14}$ atoms $\text{s}^{-1} \text{sr}^{-1}$ but with a velocity of 1300 m/s. Recently Woestenenk *et al.* [14] constructed a liquid helium cooled metastable helium beam in the 2^3S state with an average velocity of only 300 m/s and a yield of $3 \cdot 10^{12}$ metastable atoms $\text{s}^{-1} \text{sr}^{-1}$. They then further increased the intensity by a factor of 2.5 by using a hexapole magnetic lens placed in the beam line after the nozzle.

2.1.2. Electron Impact Sources

In electron bombardment sources, a well defined electron beam excites a neutral beam of atoms to metastable states. The cross-section for metastable excitation is very small ($\leq 10^{-17} \text{ cm}^2$ [22]) and therefore the overlap between the electron beam and the atomic beam is important, as is the electron beam current. The triplet excitation decreases more rapidly with decreasing electron energy than singlet excitation, therefore at low energies almost all of the metastable atoms produced are in the singlet state.

There are two different types of electron bombardment sources. The electron and atomic beams are either coaxial or transverse. Coaxial sources have a larger overlap than transverse sources but they are more complicated to build. Magnetic fields are used to confine the electrons to optimise the overlap.

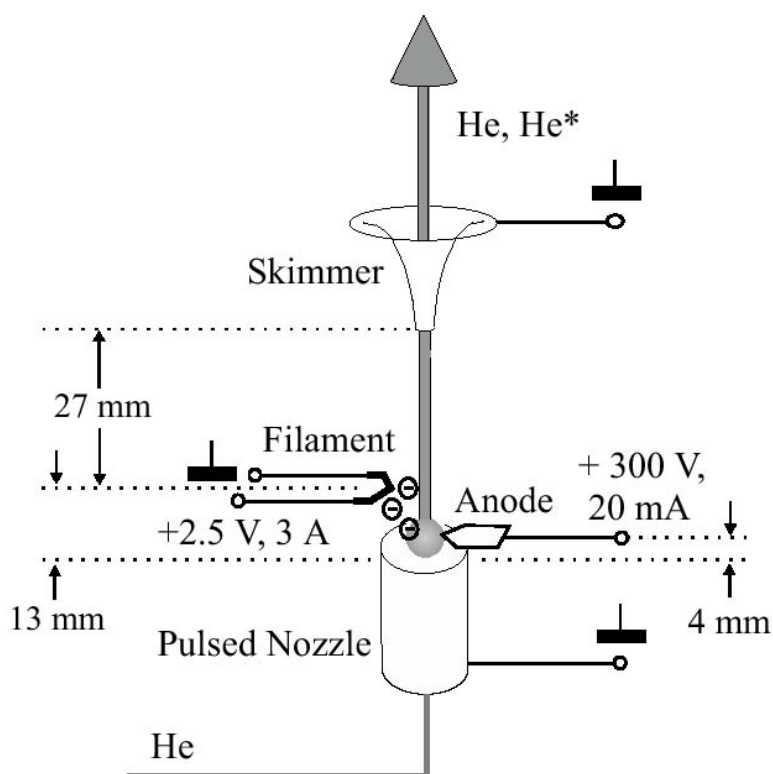


Figure 3 Schematic diagram of an electron bombardment source as used by Halfmann et al. [18]

Early designs had the disadvantage that they had a broad velocity resolution due to the momentum transfer from the electrons to the atomic beam and the initially broad distribution of the atomic beam [9, 23]. The broadening of the velocity distribution due

to momentum transfer is less for heavy species, such as argon, than for lighter species such as helium.

Recent sources use coaxial overlaps between the electron and atomic beams to reduce the velocity distribution. Additionally they used supersonic beams from pulsed discharges in combination with electron bombardment to further improve the velocity resolution [18].

2.1.3. Pulsed Discharges

Metastable helium atoms can also be created using a pulsed discharge [10, 11] without electron bombardment which simplifies the design of the source, but at the expense of intensity. The pulses can be used to examine the effect of the different components in the beam separately without the need for a chopping wheel to create a time of flight spectrum.

Yamauchi *et al.* [10] have constructed such a pulsed discharge source. They used a pulsed discharge current of up to 200 mA between a needle cathode behind a nozzle and the skimmer. A flux of $1.7 \cdot 10^{15} \text{ s}^{-1} \text{ sr}^{-1}$ was reported, however this was only during the pulse, so the time average value is much lower. This source has been used to investigate the difference in the positive ion ejection by fast He and by other species such as metastable atoms, UV photons and H^+ ions [11].

We decided not to use a pulsed discharge or electron impact source because of the complexity of the gas handling line and the need for a continuous source.

2.2. Applications of Metastable Atomic Beams

Due to their high internal energy and relatively short de Broglie wavelength, metastable rare gas atoms, and in particular helium atoms in the 2^3S_1 state, can be used in a wide range of applications. These include surface spectroscopy to measure the properties of a

metal surface [17, 24] and neutral atom lithography [25, 26, 27]. In recent years metastable helium atoms in the triplet state have been used to create Bose-Einstein condensation (BEC) [28, 29].

2.2.1. Metastable De-excitation Spectroscopy

The source designed in this work will be used in spectroscopy experiments and in later experiments will involve microscopy. Metastable de-excitation spectroscopy (MDS) has its origins in ion neutralisation spectroscopy [30], most often used to measure the properties and structure of metal surfaces. In this technique the metal surface is probed by a low energy (5-10 eV) beam of rare gas ions, typically helium. When the ions hit the metal surface, Auger neutralisation or another electron emission process occurs and an electron is ejected from the surface.

The energy spectra of the ejected electrons contain information of the electronic states at the metal surface. The energy of the ejected electron is typically less than 15 eV. Despite the low energy of the incident ions the energy spectra of the ejected electrons are broadened by the energy distribution of the ions.

A solution to this problem, which was first proposed by Delchar *et al.* [24], is the use of metastable helium atoms instead of rare gas ions. The metastable states in helium lie above the Fermi level of the metal, and therefore the excited electron in the metastable atom can tunnel into the metal when they are close enough together. This creates a helium ion immediately adjacent to the metal surface with virtually no energy other than its thermal energy (1/40 eV at room temperature). The metastable atom might also be de-excited by collision upon impact on the surface, in which case de-excitation occurs via a one electron process as opposed to a two electron process such as Auger neutralisation. Thus, the ejected electrons show virtually no energy broadening. Also, since the surface is not subject to high energy bombardment of ions anymore, sensitive adsorbed molecules may now be detected and only surface properties are examined. These processes will now be examined in more detail.

When a metastable atom impinges on a surface an electron may be ejected, depending on the work function of the metal surface and whether or not the surface is covered with an adsorbate [31, 1]. Figure 4 shows the different electron emission processes that can occur upon impact of a metastable atom on a conducting surface.

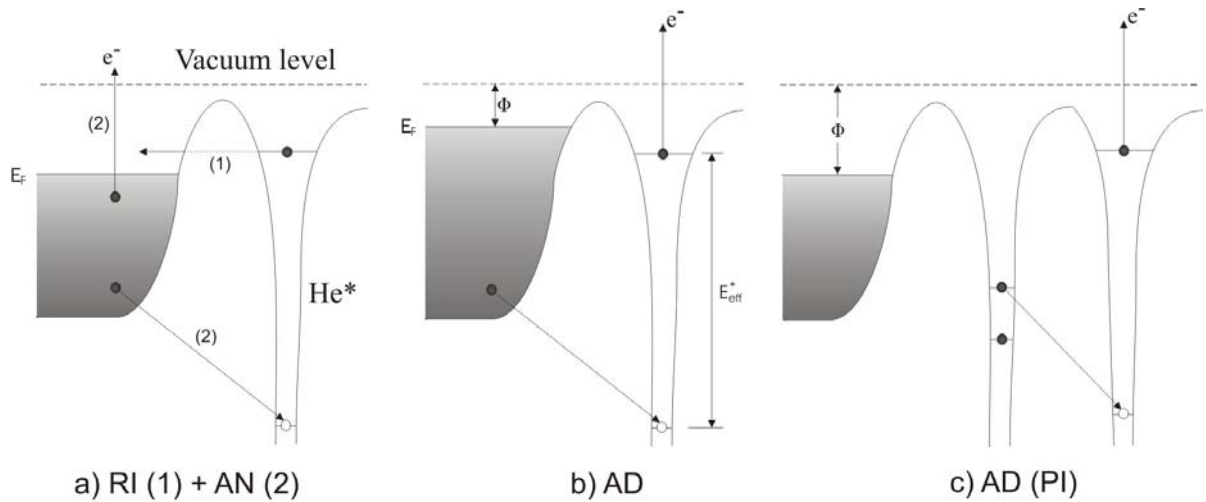
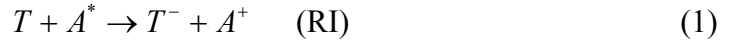


Figure 4 *Electron emission processes*

a) Resonance ionisation (RI, indicated by arrow 1) followed by Auger neutralisation (AN, arrow 2) b) Auger de-excitation (AD) c) Auger de-excitation, involving an electron from an adsorbed atom or molecule

Depending on the work function Φ of the surface electron emission from this surface upon impact of an excited atom can occur either by resonance ionisation followed by Auger neutralisation (RI + AN) or by Auger de-excitation (AD) [30, 32, 33]. When a metastable atom approaches an atomically clean conducting surface with a work function Φ , resonance ionisation occurs provided that the excited 2s helium level lies above the Fermi level E_F of the surface, and that the wave function of the 2s electron of the He^* atom overlaps sufficiently with an empty state of the surface. This results in the formation of a positive ion which continues towards the surface. If the recombination energy of this ion to neutral ground state is at least twice the work function Φ of the surface, Auger neutralisation occurs. In this case an electron tunnels into the 1s-hole of the helium ion. The energy released is then transferred to a second electron in the conduction band of the metal, which may be ejected if the energy is sufficient (see Figure 4 a). This two step process can be summarised as:



where T is the target surface and A the atom impinging on the surface.

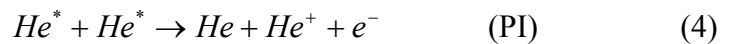
If, however, the excited 2s helium level lies below the Fermi level of the metal or if there are no vacant energy levels with a sufficient overlap with the 2s electron of the He^* atom due to, for example an adsorbate layer, resonance ionisation will be suppressed and Auger de-excitation will occur instead. In this process an electron from the conduction band tunnels into the 1s hole of the helium atom with a subsequent ejection of the 2s electron (see Figure 4 b). For Auger de-excitation to occur the effective excitation energy E_{eff}^* of the He^* atom near the surface must be greater than the work function Φ of the metal surface.



With an adsorbate layer on the metal surface the dominating process for electron emission is that of Auger de-excitation [34, 35, 36]. AD from such a surface involves an electron from the adsorbed atom or molecule which tunnels into the 1s hole of the He^* atom. A mixed behaviour has also been observed in which RI followed by AN and AD occur simultaneously [37].

For metastable helium atoms in the 2^3S and 2^1S impinging on an atomically clean metal surface with a work function $\Phi > 4.5$ eV, the resonance ionisation and Auger neutralisation process dominates [38, 39, 40].

Upon impact of a metastable atom on an insulator, Penning ionisation (PI) may occur, which is similar to AD. This is the main process occurring for free atoms in gases and is the reason why the presence of impurities causes attenuation to the He^* flux. PI can also occur between two metastable atoms:



2.2.2. Surface Magnetic Properties

The use of metastable helium beams for metastable de-excitation spectroscopy (MDS) is of particular interest in our research group. MDS can be used to measure the magnetic properties of a surface. This is performed by using spin polarised metastable helium atoms. The metastable atoms are spin polarised by using a laser with a wavelength of 1083 nm, the same optical transition that was used for laser cooling of the beam. The optical pumping will be performed in a magnetic field to define a quantisation axis [41]. The polarisation of the scattered electrons is measured to determine the origin of the electron, which can be either the incident helium atom or the surface on which the He* impinged. The magnetisation of the surface can also be determined from the de-excitation electron energy spectrum. In addition, because He* atoms are very surface sensitive, they are an ideal candidate for non destructive microscopy which could be used to map magnetic domains.

2.2.3. Microscopy

Once collimated by laser cooling, the He* beam can be used in microscopy experiments. Such a microscope was developed by Harada *et al.* [31]. In that case, the outermost surface layer was probed by flooding the sample with metastable helium atoms and (electron) optically imaging the scattered electrons with a CCD camera. This technique, however, has the disadvantage of requiring a very long acquisition time. This will be reduced by having a more intense beam. In the future, laser techniques might be developed to improve spatial resolution by focusing the He* beam into a single fine probe or an array of probes by creating an array of microlenses using standing waves. This technique has been used previously to deposit chromium atoms as a direct-write lithography process [42].

2.2.4. Neutral Atom Lithography

Metastable atoms have also been used in combination with self-assembling monolayers (SAMs) to write patterns on silicon substrates. Much of the work on this subject has

been done by Mlynek *et al.* [25, 26, 27]. The use of metastable atoms is a promising technique for lithography since it allows for nanometre resolution, large-area parallel deposition and both direct writing and resist based patterning.

Metastable noble gas atomic beams are especially suitable for lithography since they typically have a very short de Broglie wavelength of usually less than 0.1 nm which reduces diffraction, a limiting factor in UV lithography. Since metastable atoms are electronically neutral they do not suffer from electrostatic interactions, which is a limiting factor in charged particle lithography [43, 25, 44]. They also have the advantage that they are immediately quenched upon impact on a surface, and the resulting inert gas atom in its ground state can no longer damage the surface. The metastable atoms therefore only interact with the outermost atomic layer of a surface and do not damage any underlying layers of the resist. In UV lithography the damage is deep into the resist.

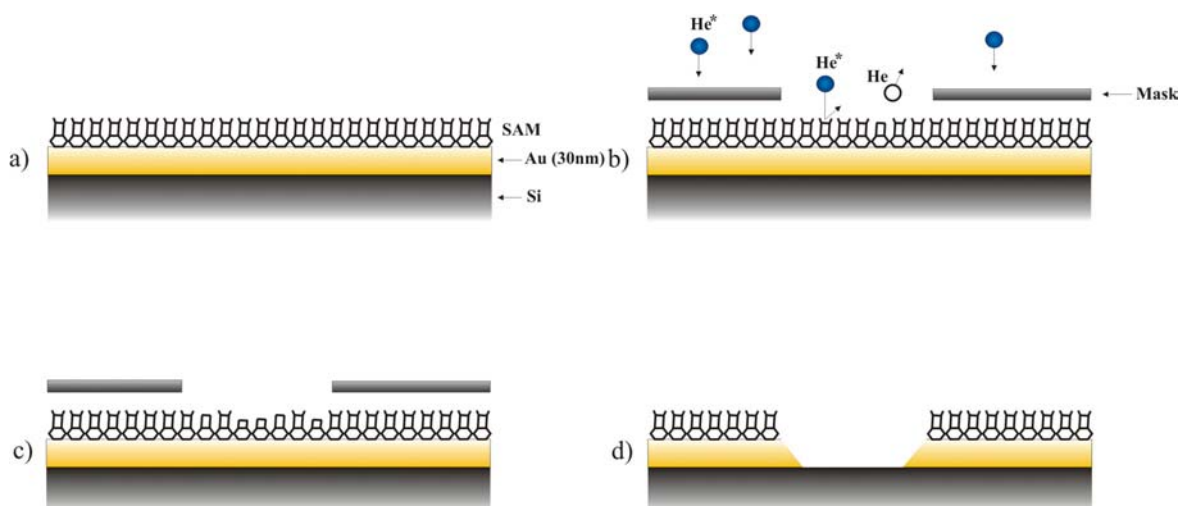


Figure 5 *The patterning process*

a) Deposition of the SAM on a gold sample b) Exposure to the metastable beam through a mask c) Metastable atoms create a damage pattern on the SAM d) The pattern in the SAM is then transferred to the gold layer by chemical etching (for more details see [27])

A self-assembling monolayer (SAM) can be used as a resist in metastable helium atom lithography since it is very thin (~1.5 nm thick). Metastable helium atoms in a small dose produce a specific pattern of damage on the SAM. This pattern can then be transferred by a wet-chemical etch onto an underlying surface such as gold [45]. When

a metastable helium atom hits the SAM, its internal energy of 20 eV is released and ionises one molecule (10 eV ionisation energy) and releases a 10 eV electron. An electron of this energy has an inelastic scattering length of about 0.8 nm [46]. Therefore a second SAM molecule in the same region will be ionised (assuming an area of 0.1 nm² per molecule). This method typically produces an edge to edge resolution of less than 100 nm [25, 47].

The patterns are produced by focusing the beam using a standing wave light field. This spatially varying light field will produce a spatially varying potential which produces a force on the atoms. In the proximity lithography experiment of Mlynek *et al.* a SAM of dodecanethiol on a gold coated silicon substrate has been used as a sample. The optimal dose giving the best contrast after etching was found to be 0.3 metastable helium atoms per SAM molecule. This was reached after an exposure of 6 min in their experiment. An edge resolution of 30 nm was also demonstrated. Bard *et al.* [43] reported a minimum dose required to damage the resist of $1.7 \cdot 10^{15}$ atoms/cm² for metastable helium which corresponds to 0.17 atoms per SAM molecule if we assume the area of the SAM molecule to be 0.1 nm². Similarly to Mlynek *et al.* they used a SAM on a gold coated silicon wafer as a sample.

2.2.5. Bose-Einstein Condensates

Most research on Bose-Einstein condensation (BEC) has been focused on alkali atoms and atomic hydrogen as these atoms can efficiently be laser cooled. Recent experiments use metastable helium atoms in the triplet state 2^3S_1 in the search for BEC [28, 29]. Laser cooling of these atoms is most often achieved by using the $2^3S_1 - 2^3P_2$ transition at 1083.3 nm. The work of reference [28] was focused on the creation and subsequent study of a BEC of $^4\text{He}^*$ atoms in the triplet state. They reported the observation of a BEC with a critical temperature of 4.7 ± 0.5 μK and a maximum number of atoms in the condensate of about $5 \cdot 10^5$. Optical absorption imaging of the atomic cloud on a CCD camera was used to determine the properties of the condensate.

2.3. Summary

Metastable helium atomic beams can be created using supersonic DC discharge sources. This is the most commonly used source and is the type of source used in this work. There are also other types of sources such as electron bombardment and charge transfer sources.

Because metastable helium atoms are very surface sensitive they can be used in various applications where very localised measurements are desired. These include neutral atom lithography, Bose-Einstein condensation and spectroscopy. The latter can be extended to microscopy experiments by using atom optic techniques to create an array of probes. Spectroscopy and microscopy are the main fields in which collimated metastable helium beams will be used in our research group.

Upon impact of a metastable atom on a metal surface an electron may be ejected either via resonance ionisation followed by Auger neutralisation, via Auger de-excitation from the surface or, in the case of surfaces covered with an adsorbate, via Auger de-excitation from the adsorbate. Which of these processes occurs depends mainly on the work function of the metal surface and the energy level occupied by the excited electron in the metastable atom. For high work functions and if the excited electron occupies a level above the Fermi level of the metal, RI followed by AN are more likely to occur. If on the other hand the work function of the metal is small, the emission process is more likely to occur via AD.

Chapter 3

Laser Cooling and the Expanding Beam

3.1. Laser Cooling

Laser cooling techniques can be used to collimate and focus the metastable beam. This technique was first used by Ashkin [48] in 1970 to deflect atomic beams. In our research group laser cooling will be used to create an intense beam of 2^3S He^* atoms. In addition, since the laser light used will only interact with atoms in the 2^3S state and not with the 2^1S atoms or the photons, which will be unaffected by the laser beam, only the 2^3S states will be focussed. Thus, after laser cooling, the beam will mainly consist of metastable helium atoms in the 2^3S state and only a tiny fraction of the beam will consist of atoms in the 2^1S state and photons because of divergence. Hence there is no need for a quenching lamp to remove the 2^1S atoms in the beam.

Light was first observed to have an effect on the motion of atoms by Frisch in 1933 [49]. In 1975 Hänsch *et al.* [50] and Wineland *et al.* [51] both independently proposed to use laser light to slow down and cool atoms. Atom optics is now a fast developing field in its own right.

The principal behind laser cooling is that an atom can experience a change in momentum when exposed to a resonant laser light. Doppler cooling is the simplest form of laser cooling and involves only two atomic states. With He^* , the two states involved are 2^3S and the 2^3P states and the transition is at 1083 nm. The laser beam is tuned to the resonance frequency of the transition between those two states.

When an atom absorbs a photon it acquires the photon momentum $\hbar\mathbf{k}_L$, where \mathbf{k}_L is the wavevector of the laser light, and $|\mathbf{k}_L| = 2\pi/\lambda$ (see Figure 6). The atom is now in an excited state and can decay either by spontaneous or by stimulated emission. If it de-excites by stimulated emission by the same laser light, the emitted photon will have the same momentum as the one that excited the atom and hence there is no net change in momentum. If, however, the de-excitation occurs via spontaneous emission there is a net change in momentum. The change in momentum due to spontaneous decay is $\hbar\mathbf{k}_S$, where \mathbf{k}_S is the wave vector of the emitted photon. The direction of the photon emitted during spontaneous emission is random with emission having the same probability to occur in every direction. Thus the expectation value $\langle\mathbf{k}_S\rangle = 0$ and therefore there is no net change in momentum during spontaneous emission. However, since there was a change in momentum as the atom absorbed the photon, the net overall effect is a change in momentum of $\hbar\mathbf{k}_L$.

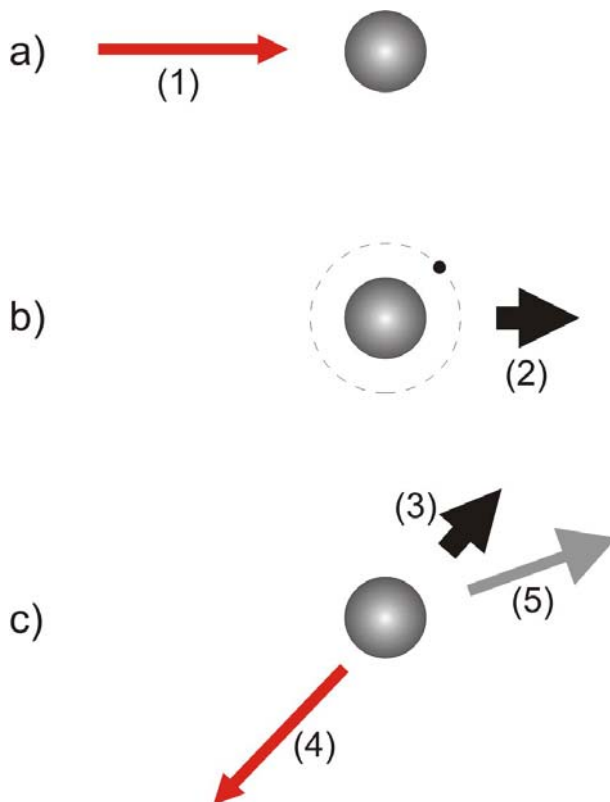


Figure 6 *Momentum transfer in spontaneous emission*

a) *The laser light (1) is absorbed by the atom* **b)** *The momentum of the photon is then transferred to the atom (2), which is now in an excited state* **c)** *Spontaneous emission occurs in a random direction (4) and the atom gains momentum in the opposite direction (3). The net effect of momentum transfer is shown by arrow (5)*

The mathematical equations giving the force on the atom when subject to laser light can be found in reference [52]. The time average force on the atom is given by:

$$F = \frac{\hbar k \Gamma}{2} \frac{s}{1 + s + (2\Delta/\Gamma)^2} \quad (5)$$

where Γ is the decay rate of the upper level, and s is the saturation parameter

$$\Delta = \delta - kv - \mu_B B / \hbar \quad (6)$$

where δ is the laser detuning, kv the Doppler shift, $\mu_B B / \hbar$ the Zeeman shift and v is the velocity of the atom.

$$k = \frac{2\pi}{\lambda} \quad (7)$$

where k is the wavenumber and λ the wavelength of the laser light, which is $1.083 \cdot 10^{-6}$ m for laser cooling of the He* (2^3S_1) atoms.

The force on the atom should be as big as possible for the laser to efficiently collimate the beam. The wavenumber k is very big, of the order of $5.8 \cdot 10^6 \text{ m}^{-1}$ and therefore the velocity distribution of the atoms in the beam must be narrow, so that a large force can be exerted on as many atoms as possible. Although this can be achieved to some extent by cooling the source with liquid nitrogen, a more significant factor is the way the gas expands as it leaves the source, and this is determined by the design of the source.

As well as having a high flux, the desirable properties of the He* beam are low velocity distributions, both transverse and longitudinal. These depend on the way the gas expands from a high pressure region into a vacuum and can occur in two different ways, depending on the relationship between the mean free path of the gas particles in the reservoir and the dimension of the nozzle orifice. The mathematical derivations in the following section are taken from reference [53].

3.2. Jet Theory

3.2.1. Effusive Beams

Effusive beams are created when the diameter of the nozzle orifice D is much smaller than the mean free path λ_0 of the gas particles in the reservoir. This corresponds to a molecular flow. The particles in such a beam suffer almost no collisions as they expand into the vacuum.

The velocity distribution of such a beam is given by the equation

$$P(v)dv = \frac{m^2}{2(RT_0)^2} v^3 \exp\left(-\frac{mv^2}{2RT_0}\right) dv \quad (8)$$

where m is the molar mass of the gas particles and T_0 is the reservoir temperature [54, 55]. Note that this is somewhat different to the Maxwell-Boltzmann distribution for the same temperature (Figure 7). The velocity distribution in an effusive beam only depends on m and T_0 and is independent of the pressure inside the reservoir and is not altered by the presence of other species. In the current work D/λ_0 is usually greater than 50 for nozzle diameters ranging from 0.15 mm and 0.35 mm (see section 4.1.2 for the calculation of λ_0) so one must take into account the intermolecular interactions as described below.

3.2.2. Supersonic Expansions

A supersonic Jet is formed when the mean free path of the molecules in the reservoir, λ_0 , is much smaller than the diameter of the nozzle orifice, D . This will be the case for the nozzle of the source used in this work, and the flow is said to be in the continuum regime. The particles then suffer many collisions as they expand into the low pressure region, and the expansion is therefore governed by gas dynamic equations. Assuming an ideal gas and neglecting viscous and heat conduction effects the terminal velocity can be determined. The flow is assumed to be a reversible and adiabatic process, and thus the state of the gas changes isentropically. The density of the gas will gradually

decrease inside the small nozzle and the flow changes from a continuum to a molecular flow, at which point the collision rate will tend to zero.

Since the expansion can be regarded as adiabatic, the enthalpy is almost completely converted into directed mass flow, which leads to beams with very low internal temperatures but with high translational velocities. The velocity distribution is approximately Maxwellian. Since the internal temperature is low the distribution is very narrow.

The enthalpy of the system is conserved and is given by the equation based on the first law of thermodynamics

$$H + \frac{1}{2}mv^2 = H_0 \quad (9)$$

where H is the molar enthalpy of the gas and H_0 is the total enthalpy of the system which is a constant [56]. v is the average flow velocity and m the molar mass of the particles.

For an ideal gas $dH = C_p dT$, where C_p is independent of temperature.

Therefore the final flow velocity v_{\max} is given by

$$v_{\max} = \sqrt{\frac{2H(T_0)}{m}} = \sqrt{\frac{2C_p T_0}{m}} \quad (10)$$

where $H(T_0)$ is the molar enthalpy of the gas at the temperature of the reservoir, T_0 , and m is the molar mass.

For ideal monatomic gases $C_p = \frac{5}{2}R$.

An adiabatic and isentropic expansion of an ideal gas from a reservoir with (p_0, T_0, ρ_0) into a low pressure region with (p_1, T_1, ρ_1) is governed by the equations

$$\frac{T_1}{T_0} = \left(\frac{p_1}{p_0} \right)^{(\gamma-1)/\gamma} \quad (11)$$

$$\frac{\rho_1}{\rho_0} = \left(\frac{p_1}{p_0} \right)^{1/\gamma} \quad (12)$$

and

$$\frac{\rho_1}{\rho_0} = \left(\frac{T_1}{T_0} \right)^{1/(\gamma-1)} \quad (13)$$

where p is the pressure, T the temperature and ρ the density of the gas. γ is the heat capacity ratio C_p/C_v , which equals 5/3 for monatomic gases. These equations are important as they characterise the quality of the beam in terms of parameters that we can control. They predict that a higher pressure ratio, of the pressure p_0 in the source to the pressure p_1 in the source chamber, will reduce the temperature during a supersonic expansion.

For these equations to hold the expansion must take place in continuum flow and must be adiabatic, isentropic and follow ideal gas behaviour. These equations would break down in molecular flow regime.

3.2.3. The Mach Number

The Mach number M is defined as the average flow velocity $v(x)$ over the local speed of sound $a(x)$ at position x :

$$M(x) = \frac{v(x)}{a(x)} \quad (14)$$

and

$$a(x) = \sqrt{\frac{\gamma k_B T(x)}{m}} \quad (15)$$

where k_B is the Boltzmann constant and m the mass of the particles.

According to equation 11 a larger pressure ratio leads to higher cooling during the expansion, thus reducing the local speed of sound while the average flow velocity increases as random motion is converted into directed mass flow. The expansion is called supersonic when the Mach number exceeds unity.

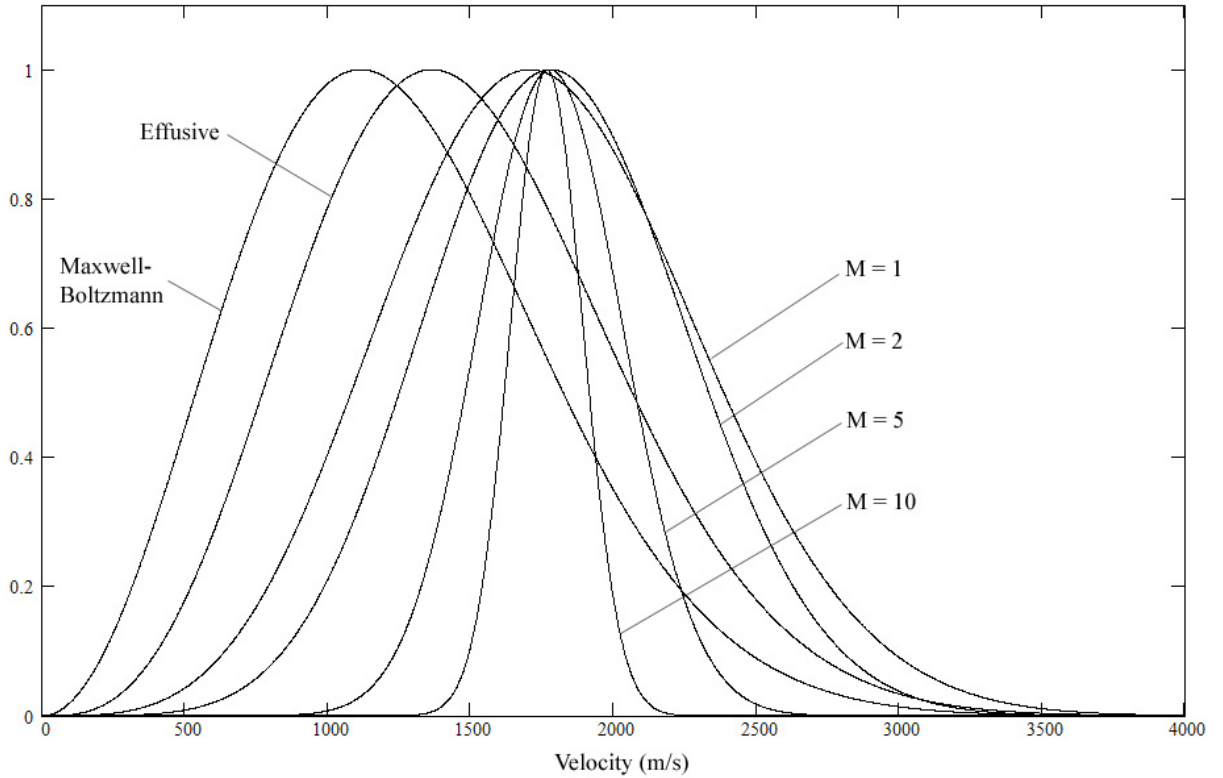


Figure 7 Velocity distributions for different Mach numbers for He at 300K

The velocity distribution for a supersonic expansion is a Gaussian distribution and is given by the equation

$$P(v) = Av^3 \exp\left[-\frac{m(v - v(x))^2}{2RT(x)}\right] \quad (16)$$

where $v(x)$ is the average flow velocity, $T(x)$ the local temperature in the expanded beam and A is a normalisation factor. The Maxwell-Boltzmann distribution, shown in Figure 7, gives the thermal distribution of the particles inside the source. The

temperature $T(x)$ is dependent on the source temperature T_0 and the Mach number and is given by

$$T(x) = T_0 \cdot \left[1 + \frac{\gamma - 1}{2} M(x)^2 \right]^{-1} \quad (17)$$

The velocity distribution for a supersonic expansion can now be calculated using equations 16 and 17, and a graph of the number density of the particles at a given velocity is shown in Figure 7 for different Mach numbers. The velocity distribution gets narrower with increasing Mach number, for a constant source temperature. An increase in temperature has the effect of increasing both average flow velocity and velocity width for a given Mach number.

3.3. Summary

The expansion of a gas from a high pressure region into a vacuum can either form an effusive beam or a supersonic beam. Which of these beams will be created depends on the relationship between the mean free path of the gas particles and the dimensions of the nozzle orifice. An effusive beam is formed when the diameter of the nozzle orifice is much smaller than the mean free path of the gas, whereas a supersonic expansion occurs when the orifice is much bigger than the mean free path. The velocity distribution of a supersonic beam is much narrower than that of an effusive beam, the latter however has a smaller average flow velocity. The expansion is called supersonic when the Mach number, which is defined by the average flow velocity over the local speed of sound, exceeds unity.

Chapter 4

Experimental Setup

4.1. Vacuum System

4.1.1. Vacuum Chamber Arrangement

The vacuum system was built up from components salvaged from other experiments. It consists of two separate chambers (Figure 8) connected by an aperture (skimmer). It is advantageous to skim the beam so that it can be transmitted into a second chamber with a much lower pressure. A low background pressure of typically less than 10^{-4} mbar is maintained in the source chamber by using a diffusion pump (Edwards Vapour pump E04) in combination with a turbo molecular pump (Edwards EXT 250M) (see Figure 8). The pumping speed of the diffusion pump with its liquid nitrogen trap is approximately 300 l s^{-1} for helium. The EXT 250M has a pumping speed of 250 l s^{-1} for nitrogen and 240 l s^{-1} for helium.

To decrease the partial pressure of water, resulting from water being adsorbed to the walls of the gas line from the helium cylinder to the source, a cold trap filled with liquid nitrogen is added. The driving pressure is then control by a needle valve on the gas line between the cold trap and the source. The pressure in the source chamber was measured with a Penning gauge, whereas the pressure in the second chamber was measured with an ion gauge. A residual gas analyser (ANAVAC 2) could be connected to either of the chambers to measure the partial pressures of the residual gases.

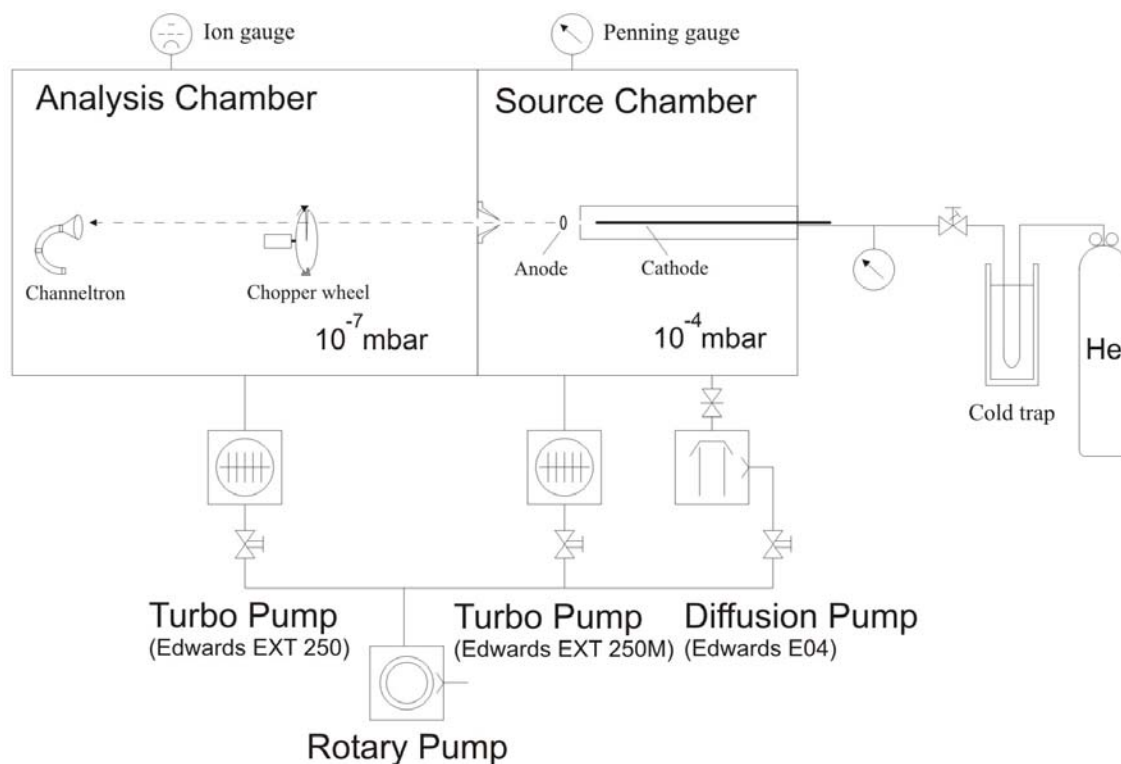


Figure 8 *Vacuum chamber arrangements*

The vacuum system is differentially pumped in order to achieve a much lower pressure in the second chamber. The aperture separating the source chamber from the second chamber allows it to be maintained at a much lower pressure (less than 10^{-6} mbar). A second 250 l s^{-1} turbo pump (Edwards EXT 250) is connected to the second chamber. The analysis of the metastable beam is performed in the second chamber.

The diffusion pump and the two turbo pumps are all connected to the same backup pump (Edwards E2M40). The diffusion pump can be closed off from the rest of the vacuum system by a gate valve. This way the vacuum chamber can be let up to atmospheric pressure without having to shut off the diffusion pump. Only the two turbo pumps need to be turned off before letting the system up to air.

4.1.2. Differential Pumping and Pumping Speeds

The mean free path of helium depends on the temperature and the pressure in the chamber. The mean free path, λ is given by the equation

$$\lambda = \frac{1}{n\sqrt{2\pi}d^2} = \frac{kT}{\pi\sqrt{2}Pd^2} \quad m \quad (18)$$

where d is $2.15 \cdot 10^{-10}$ m for helium, and n is the number density and can be deduced from the equation $p = nkT$.

At 50 mbar and 300K the mean free path for helium is $4 \cdot 10^{-6}$ m. Thus, it is much smaller than the size of the nozzle (~ 0.15 mm), and the flow is in the viscous regime and hence a supersonic jet is created after the nozzle. In the source chamber outside the source, the pressure is around 10^{-4} mbar and the temperature about 300K. The mean free path for helium in this chamber is $\lambda = 2$ m. The skimmer between the source chamber and the analysis chamber has a diameter of approximately 1 mm. The beam passing through the skimmer is therefore in the molecular flow regime.

During the design stage this was analysed using methods in reference [57] and is summarised below. The optimal pressures in the chambers are better than 10^{-4} mbar for the source chamber and about 10^{-7} mbar for the analysis chamber, so that high voltage electron multipliers can be used. To calculate the size of the aperture needed to achieve such pressures the throughput of gas from the source and the diameter of the nozzle must be known. Typically the driving pressure inside the source is around 40 mbar, depending on the size of the aperture used.

The throughput of the pump connected to the source chamber can also be deduced from the nozzle dimensions, the driving pressure inside the source and the pressure in the source chamber. For a nozzle orifice $d = 2.5 \cdot 10^{-2}$ cm in diameter and $l = 0.18$ cm in length (see Figure 9), the conductance is given by the following equation, for He:

$$C_1 = \frac{12.4 \cdot \alpha \cdot d^3 / l}{1 + 4 \cdot d / (3l)} \quad l \cdot s^{-1} \quad (19)$$

where d and l are in cm and the scaling term $\alpha = 0.2$ for He ($\alpha = 1$ for N_2)

This is correct for molecular flow and is therefore a conservative estimate by possibly tens of percent since the flow inside the source is in a continuum regime and only changes to a molecular flow as it expands through the nozzle.

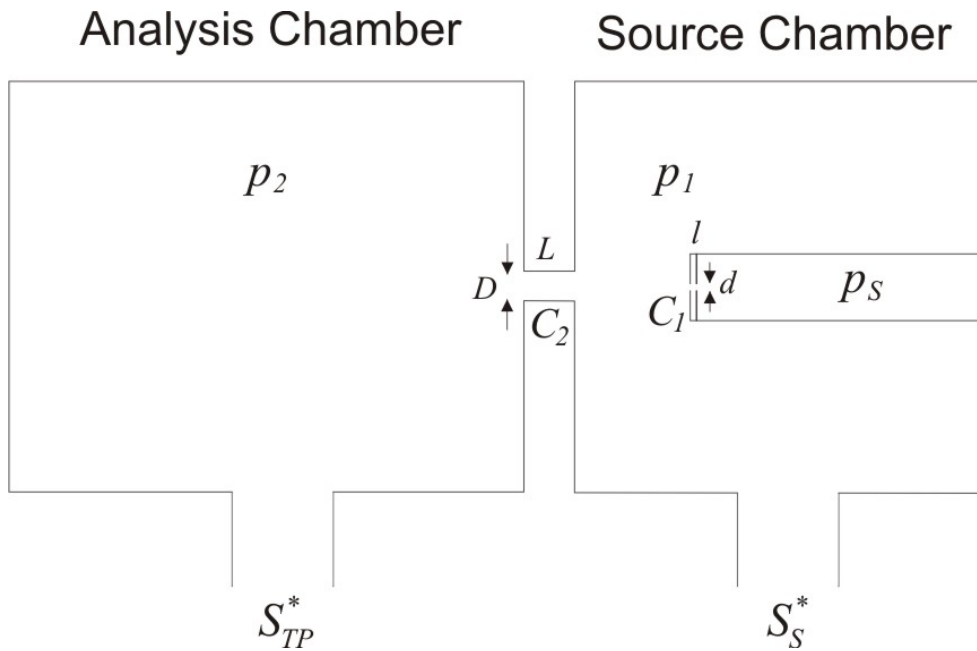


Figure 9 Pressures in the system

This gives a conductance of the nozzle of approximately $C_1 = 9 \cdot 10^{-4} \text{ l} \cdot \text{s}^{-1}$. The throughput is defined by the conductance times the difference in pressure.

$$Q = C(p_s - p_1) \text{ mbar} \cdot \text{l} \cdot \text{s}^{-1} \quad (20)$$

where p_s and p_1 are the pressures in the source and in the source chamber respectively and the pressures are given in mbar. This gives a throughput of $Q = 0.036 \text{ mbar} \cdot \text{l} \cdot \text{s}^{-1}$.

The pumping speed is given by the throughput divided by the pressure in the chamber. Considering that almost all the gas from the source is evacuated by the pump and only a tiny fraction goes through the aperture between the two chambers, the required pumping speed is given by:

$$S_S^* = Q/p_1 \text{ l} \cdot \text{s}^{-1} \quad (21)$$

For a throughput of $0.036 \text{ mbar} \cdot \text{l} \cdot \text{s}^{-1}$ and a pressure of 10^{-4} mbar in the source chamber, the required pumping speed $360 \text{ l} \cdot \text{s}^{-1}$. Thus, to achieve a pressure of 10^{-4} mbar with a

nozzle diameter of 0.25 mm and a driving pressure of 40 mbar, a pump with a pumping speed of at least $360 \text{ l}\cdot\text{s}^{-1}$ is needed.

For an aperture of 0.35 mm the required pumping speed is $940 \text{ l}\cdot\text{s}^{-1}$. Therefore a second pump in addition to the diffusion pump was added. Since the only available port on the source chamber was on the top, the pump needed to be placed upside-down. The only pump that was able to operate at this angle was a magnetic bearing turbo molecular pump with a pumping speed of $250 \text{ l}\cdot\text{s}^{-1}$ (Edwards EXT 250M).

The dimensions of the aperture between the source chamber and the analysis chamber can also be calculated using equations 19 and 20. The pressure in the analysis chamber should be around 10^{-7} mbar in order to be able to operate a channel electron multiplier (channeltron) and to reduce collisions between the atoms in the beam to a negligible level.

The pumping speed of the turbo pump, S_{TP}^* is related to the conductance of the aperture by the following equation:

$$S_{TP}^* \cdot p_2 = C_2(p_1 - p_2) \quad \text{mbar} \cdot \text{l} \cdot \text{s}^{-1} \quad (22)$$

where p_1 and p_2 are the pressures in the source chamber and the analysis chamber respectively. C_2 is the conductance of the aperture between those two chambers (see Figure 9). The pumping speed S_{TP}^* is that of the turbo pump (Edwards EXT 250) and is $250 \text{ l}\cdot\text{s}^{-1}$.

This gives a value for the conductance C_2 of $0.25 \text{ l}\cdot\text{s}^{-1}$. For short pipes the conductance can be evaluated using Dushmann's equation:

$$C = 12.4 \cdot D^3/L - \frac{4}{3} \frac{D}{L} \quad \text{l} \cdot \text{s}^{-1} \quad (23)$$

From equations 22 and 23 and putting the length L to 2 mm, the dimensions of the aperture can be calculated. To get a pressure of 10^{-7} in the analysis chamber the aperture must be approximately 0.2 mm in diameter and 2mm in length.

4.2. Source Design

4.2.1. Design Enabling Changes of Operating Parameters

The metastable helium source used in this work was designed so that properties such as the distance between the cathode and the anode, the size of the nozzle or the size of the pyrex tube constraining the discharge could easily be changed. To be able to do so, no cooling system was included in the design of the source. This means that the velocity of the beam will be high, but this source will enable us to investigate the change in translational velocity and velocity distribution when changing different parameters. The changes will then also apply to sources cooled by liquid nitrogen for instance.

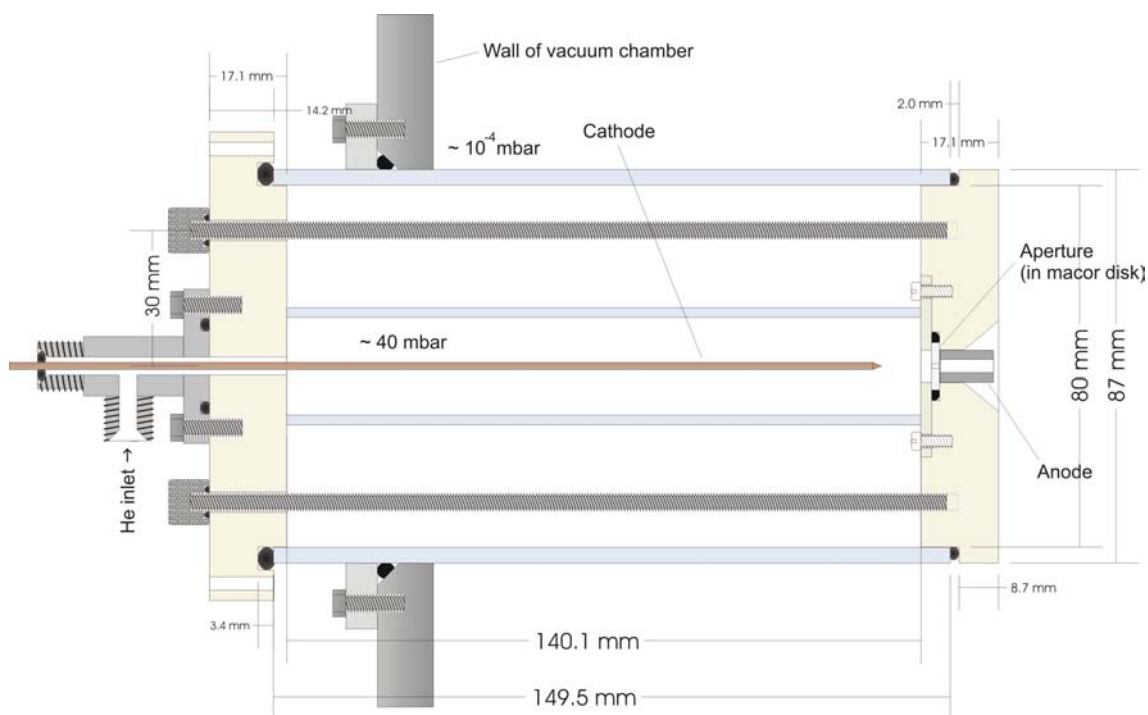


Figure 10 *Schematic diagram of the source used in this work*

The nozzle is made out of machinable ceramic (macor) as this is a very robust insulator with a minimal wear when placed in a discharge. Nevertheless the macor disk needs to be changed after a few hours of continuous operation of the discharge in order to get reproducible results, as the macor disk still wears off and the diameter of the aperture increases slightly during extended operation.

The source is designed so that the macor disks can be replaced easily and different aperture sizes can be tested. This aperture needed to be the only way the gas inside the source could escape to the source chamber. For this reason an O-ring was placed around the aperture disk and the two were then held down by a second, bigger macor disk (see Figure 10). The only material in the vicinity of the discharge was macor, which is a very good insulator with a good mechanical strength and hence does not influence the discharge.

The cathode was made of tungsten and was ground at one end to form a sharp tip. This increases the local charge density, thus enhancing the electric field and making the discharge easier to strike. To centre the cathode with respect to the nozzle orifice, a nylon piece is placed inside the pyrex tube with a small hole in the middle to hold the cathode and a few holes around to let the helium through. The distance between the cathode and the nozzle can be changed by simply pushing the anode in or pulling it out, although care must be taken that the discharge is off at that time to avoid electrical shocks. The advantage of this design is that the position of the cathode can be changed without having to let the system up to air. This greatly reduces the error in the measurement since the parameters are kept constant. The source was held together by three stainless steel studdings.

In an early design the anode was made of a small stainless steel ring placed about 15mm away from the nozzle. However, to strike and maintain a stable discharge a very high voltage of about 5000 V was needed. The lowest voltage at which a discharge was running, at a driving of 70 mbar, was 3000 V between cathode and anode. In a later design the anode was a stainless steel tube, which was placed directly behind the nozzle. This greatly improved the yield of metastable atoms, while at the same time it drastically reduced the voltage needed to run the discharge.

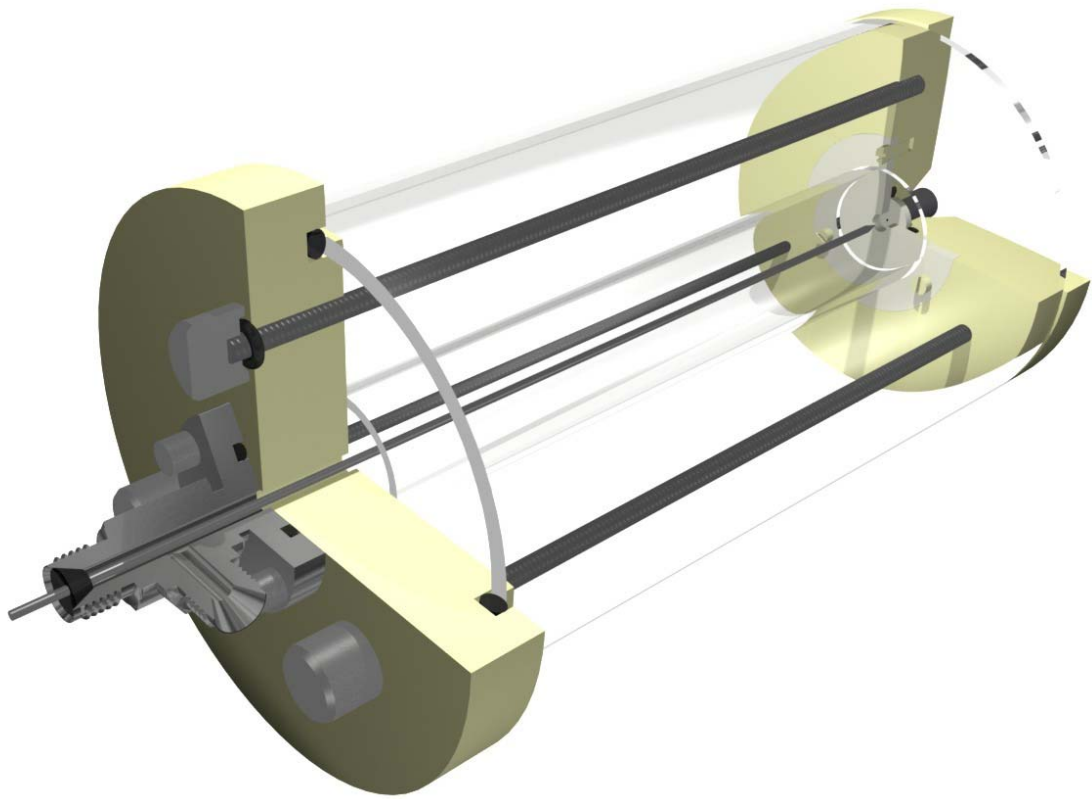


Figure 11 *Cross sectional view of the He* source used in this work*

The yellow parts are nylon and the white parts macor. The parts represented in grey are stainless steel except for the needle cathode which is made of tungsten. The components in black represent O-rings.

With small nozzles, below 0.25 mm in diameter, it was quite difficult to start the discharge, and a very high voltage and a high driving pressure were needed to initiate it. To make it more easy to strike the discharge, a metal disk with a hole bigger than that of the nozzle was placed between the aperture disk and the cathode. This disk was connected to one of the metal studdings, which could be grounded from outside the vacuum system. An initial discharge was then struck between this disk and the cathode. This discharge was very easy to strike since it was entirely inside the source and not obstructed by any aperture. The anode was then put at a potential and when the metal disk was disconnected from ground, ie floating, the discharge then only went from the cathode to the anode.

4.3. Operation of the Source

4.3.1. Electrical Circuitry

A schematic diagram of the electric circuitry of the source is shown in Figure 12. Two power supplies are used to create the DC discharge. The cathode is at a negative potential and is connected to a 5 kV (maximum) power supply through a 150 k Ω ballast resistor. This resistor is used to stabilise the discharge and to protect the power supplies. The anode is connected to a 1500 V (maximum) power supply and is at a positive potential with respect to ground.

The discharge is started by applying a high voltage to the electrodes for a short period of time. The voltage needed to start the discharge depends on the pressure in the source, the distance between cathode and anode and the size of the aperture.

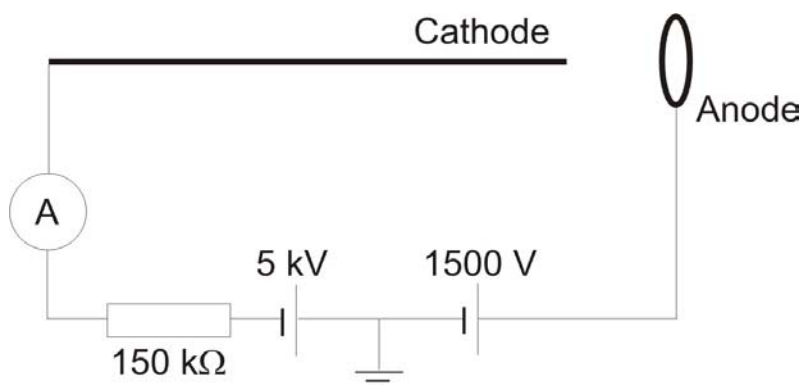


Figure 12 *Schematic diagram of the electric circuitry of the source*

Typically, the voltage applied to the electrodes and the ballast resistor was between 600 V and 1800 V (adding the voltages of both power supplies together) giving a discharge current of 2 mA to 10 mA respectively. The discharge current and the He^{*} yield are dependent on both voltage and pressure. This is discussed in more details in chapter 5.

4.4. Measurement of the Properties of the Beam

4.4.1. Removal of Unwanted Components from the Beam

A few centimetres downstream from the anode a skimmer (the aperture between the source chamber and the analysis chamber) collimates the beam. The geometry of the skimmer is quite crucial and can have an important effect on the divergence of the beam [7]. The distance between the aperture of the source and the skimmer is also of importance, since the metastable atoms have an increasing chance to be de-excited to ground state via collisional processes (Penning) with increasing aperture-skimmer distance. The distance depends on the type of source used and is usually around 5 mm for DC discharge sources [6, 10] and is about 30-40mm for electron impact sources [18].

A distance of about 30 cm between the source and the detector is usually enough to remove the short lived (non-metastable) excited atoms. The charged particles in the beam can be removed by an electric field created by metal plates at a potential or by a charged grid placed between the anode and the skimmer.

In the case of helium where there are two long lived metastable states (2^1S_0 and 2^3S_1) the singlet state can be removed by optical quenching. This can be achieved by photon excitation of this state to higher singlet levels, which then decay preferentially to the ground state [9, 58, 59]. In order to quench the singlet component of the beam a spirally shaped He discharge lamp could be used. In this work no quenching lamp has been used and the ratio of triplet to singlet state has been taken from previous work, where the 2^3S_1 state was found to be 8 times as populated as the 2^1S_0 state [13].

4.4.2. Electron Emission Method

To measure the intensity of the metastable atomic beam, the electron emission method may be used. When a metastable atom collides with a surface the probability of an electron being emitted by one of the mechanisms described in section 2.2.1 is very high and is usually greater than 70%, depending on the surface properties [60]. A simple detector consists of two metal plates, one at a positive voltage and the other at ground.

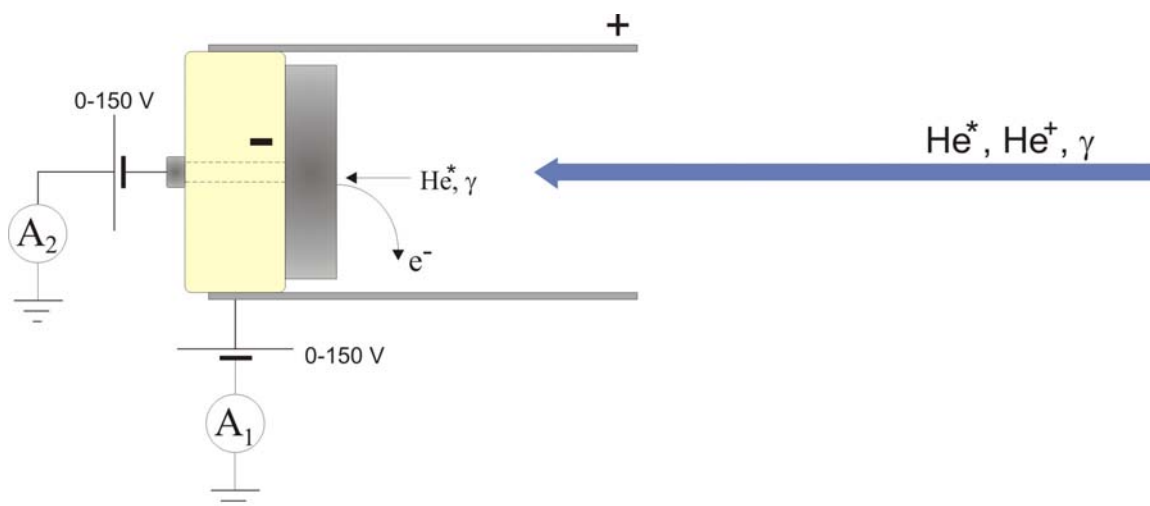


Figure 13 *Metastable detector*

If a metastable helium atom hits the grounded metal plate the ejected electron will then be attracted to the positive plate, and the current reading on this plate is directly proportional to the number of metastables incident on the plate. However, electrons arising from the impact of electrons or UV photons on the grounded plate are also recorded and metastable helium atoms in both 2^3S_1 and 2^1S_0 states are detected. A_1 measures the current on the outer sheath of the detector. This will give a measure of the metastable atoms and photons impinging on the deflector. A_2 will measure photons and metastable atoms (as a loss of electrons) as well as positive ions that are collected the inner metal disk. These are minimised by a retarding grid behind the anode, set to 30-40V above the anode voltage.

For a skimmer diameter of d , anode to skimmer distance of L_1 and a skimmer to detector distance of L_2 (see Figure 14), the area A of the beam that hits the plate is given by

$$A = \pi \cdot \left(\frac{L_1 + L_2}{L_1} \frac{d}{2} \right)^2 \quad (24)$$

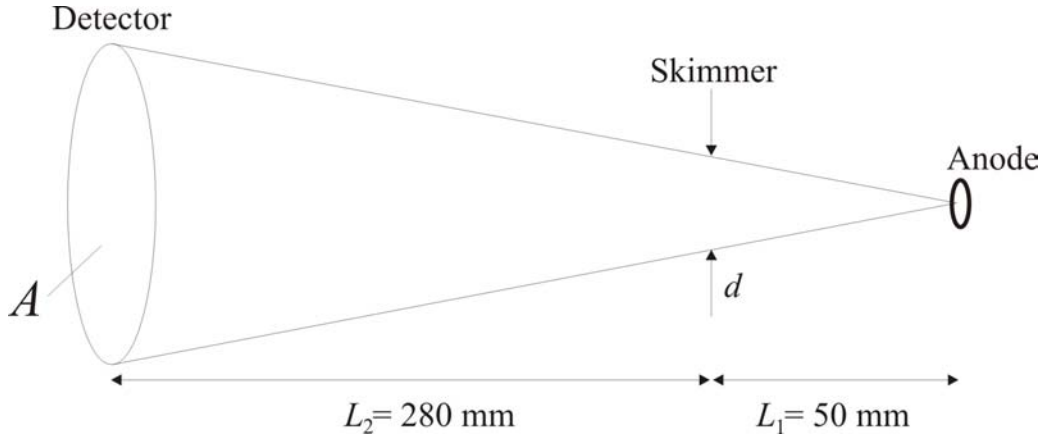


Figure 14 *Dimensions of the system*

Let N be the number of metastable atoms hitting the detector each second. If the efficiency of a metastable atom hitting the plate and emitting an electron is 70% [60], the measured current is simply the number of He^* atoms hitting the plate each second, N , times the charge per electron, e , scaled by the efficiency factor. The ratio of 2^3S atoms to the combined 2^1S atom and photon contribution must also be taken into account and is 0.9 as found in previous work [18].

$$I = N \times e \times \text{efficiency} = 1.6 \times 10^{-19} \times \frac{0.7}{0.9} \times N \quad (25)$$

The flux of He^* , given in $\text{atoms} \cdot \text{s}^{-1} \cdot \text{sr}^{-1}$, is then given by the $N \times R^2 / A$, where A/R^2 is the solid angle of the beam (for $A \ll R^2$) and R is the distance anode-detector, ie $R = L_1 + L_2$.

Therefore, for a measured current of I Amperes on the plate, the flux is

$$\text{Flux} = 8 \times 10^{18} \frac{I \times R^2}{A} \text{ atoms} \cdot \text{s}^{-1} \cdot \text{sr}^{-1} \quad (26)$$

Putting the values of $L_1 = 50$ mm and $L_2 = 280$ mm and a skimmer diameter of $d=3$ mm, the metastable flux is therefore $2.8 \cdot 10^{12}$ $\text{atoms} \cdot \text{s}^{-1} \cdot \text{sr}^{-1}$ per nA.

4.4.3. Time of Flight Technique

The velocity distribution of the beam can be measured by the time of flight technique. To detect the metastable atoms and UV photons a channel electron multiplier (channeltron) is placed in line with the beam axis. The channeltron is placed in the analysis chamber which is situated after the skimmer. A chopper wheel with a slit of less than 1 mm is placed in this chamber between the skimmer and the channeltron along the beam axis (Figure 15). The chopper wheel spins at about 60 Hz. Every time the slit passes through the beam line, photons and metastable atoms can pass through and reach the channeltron after a short delay, which depends on the velocity of the particles and the distance between the chopper wheel and the detector. Photons will reach the channeltron almost immediately. The metastables though are much slower and therefore will only reach the channeltron after a short time given by their velocity. The faster the metastables the earlier they will reach the channeltron. By using the photon peak as the zero point and knowing the distance between the chopper wheel and the channeltron, the velocity distribution can be worked out.

$$v = \frac{d}{TOF} \quad m \cdot s^{-1} \quad (27)$$

where v is the velocity of the He^* atoms in $m \cdot s^{-1}$, d is the distance in metres between the chopper wheel and the channeltron and TOF is the average time of flight of the He^* atoms in seconds measured from the maxima of the velocity distributions. The distance between the chopper wheel and the channeltron in this experiment is 0.45 m.

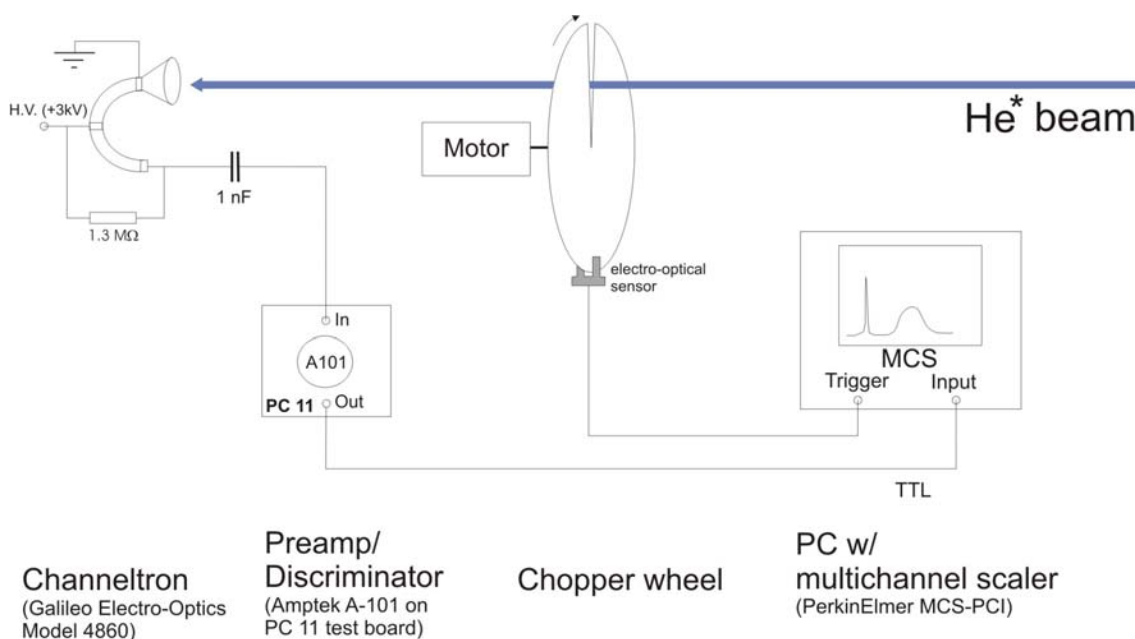


Figure 15 Schematic diagram of the TOF technique

A slit is placed in front of the channeltron to increase the timing resolution of the measurement. It also prevents the device from being saturated by the (briefly) high signal.

When a metastable atom or a UV photon hits the channeltron, secondary electrons are created which are then accelerated and amplified to the back of the channeltron by a voltage of 3 kV. The pulses created this way are then amplified and fed into a multichannel scaler (MCS). The MCS stores those pulses in different time channels and adds the so obtained distribution to the previous one each time the slit of the chopper wheel passes through the beam line. The dwell time, the counting time in each channel is typically set to around 1 μ s. Each sweep of the MCS is triggered by an electro-optical sensor which provides a triggering signal each time a hole in the chopper wheel passes between the light and sensor. The hole in the chopper wheel is placed such that when it rotates past the trigger the slit in the chopper wheel passes through the beam line a short time afterwards in order to minimise any effect of the wheel spinning irregularly.

A chopper wheel is only needed for DC discharge sources, and is often omitted in pulsed sources as the latter use the pulses to differentiate between different velocity distributions.

4.5. Summary

The vacuum system is differentially pumped with the beam being skimmed before it enters the analysis chamber. The pressure in this chamber is much lower than in the source chamber, around 10^{-7} mbar, and therefore the properties of beam can be measured in this chamber. A channel electron multiplier is used in combination with a chopper wheel to measure the velocity distribution of the beam. This is known as the time of flight (TOF) technique and will provide the analysis of the average flow velocity as well as the velocity distribution. In addition it will give the relative proportion of photons to the metastable components in the beam. Once these are known, the electron emission method will provide a simpler measure of the yield of metastables. The source was designed in such a way that many parameters could be investigated at the expense of design simplicity. It is expected that a better understanding of these parameters will lead to a simpler design for future experiments.

Chapter 5

Results and Discussion

Many results have been taken, but only a selection will be given here, aimed at providing an overview of how different factors influence the quality of the beam. Figure 16 shows a typical time of flight spectrum. The first peak is the photon peak, which marks the zero of the time of flight. The shape of the photon peak is due to the fact that the beam passes through the slit for a finite time. The resolution of the instrument is given by the width of this peak. The second peak is due to the metastable atoms. The velocity distribution of He^* atoms, obtained using equation 27 is given in Figure 17. The distribution is approximately symmetric, so the velocity at the peak can be described as the average velocity.

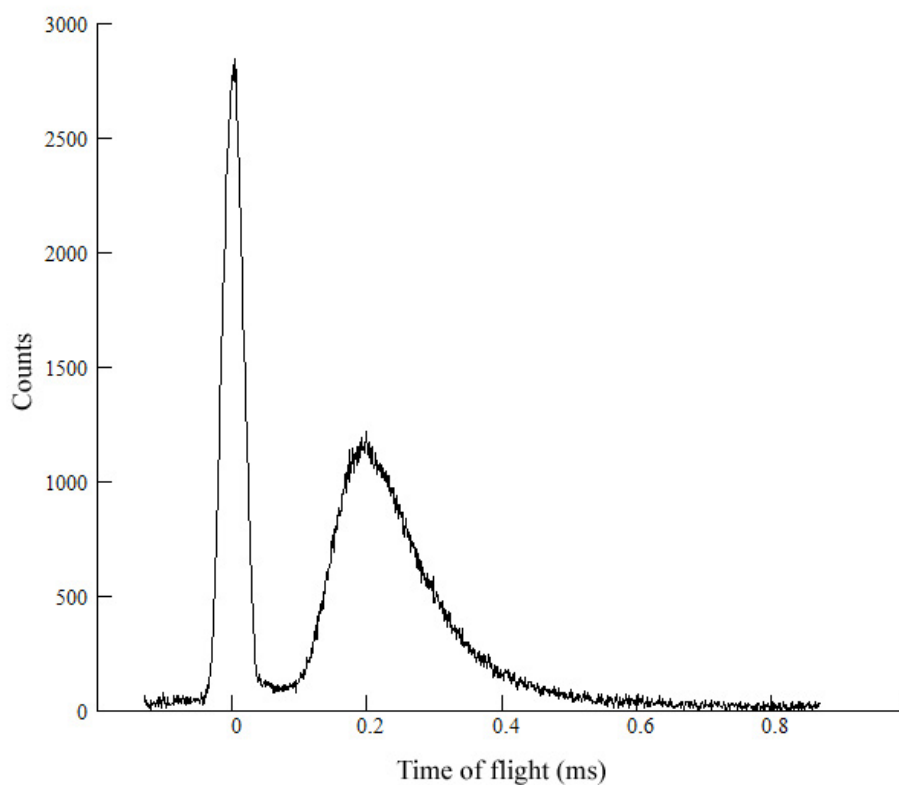


Figure 16 *Typical time of flight spectrum*

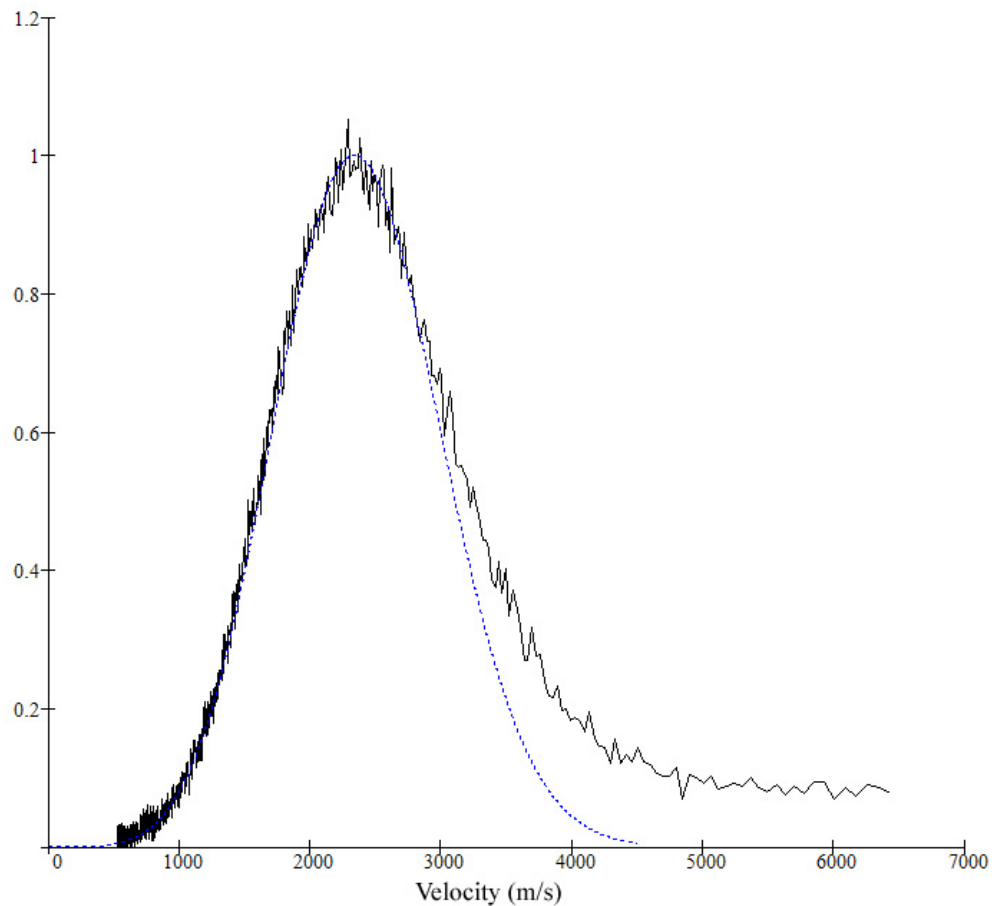


Figure 17 *Velocity distribution of metastables*

A calculated distribution (dotted curve) was fitted to the data, which gave a source temperature of 520 K and a Mach number of 2.5 in this case. The calculated distribution first needed to be convoluted with the photon distribution before comparing it to the measured data. The discrepancy at high velocities is possibly due to the presence of fast neutrals and residual ions

The above figure shows the metastable distribution (solid line) with the closest fitting calculated distribution (dotted curve), obtained using equation 16. As can be seen in Figure 7, the average velocity does not change by a great amount for different Mach numbers in a supersonic expansion. The average velocity is primarily dependent on the temperature in the source. The Mach number on the other hand is independent of temperature, and as the Mach number increases, the distribution gets narrower. Note that a lower temperature also leads to a narrower distribution.

The calculated distribution can therefore be fitted to the experimental data by first setting the temperature so that the average velocities overlap. Knowing the temperature in the source, the Mach number was changed until the two distributions have the same width.

5.1. Beam Flux

The flux of metastable atoms is largely determined by the behaviour of the discharge. Apart from geometry, the parameters which can be varied are the driving pressure and the discharge voltage or current. In the following graphs the flux is given as either counts or nA (which can be converted to $s^{-1}sr^{-1}$ using equation 26) depending on whether the TOF or electron emission detector was in place at the time.

5.1.1. Influence of Discharge Current on He* Yield

The effect of the discharge current on the metastable yield is shown in Figure 18. These measurements were performed with a nozzle diameter of 0.25 mm, a pressure in the source chamber of $3 \cdot 10^{-5}$ to $4 \cdot 10^{-5}$ Torr and a driving pressure of 60 mbar (square/red dots in Figure 18) and 35 mbar (diamond/blue dots).

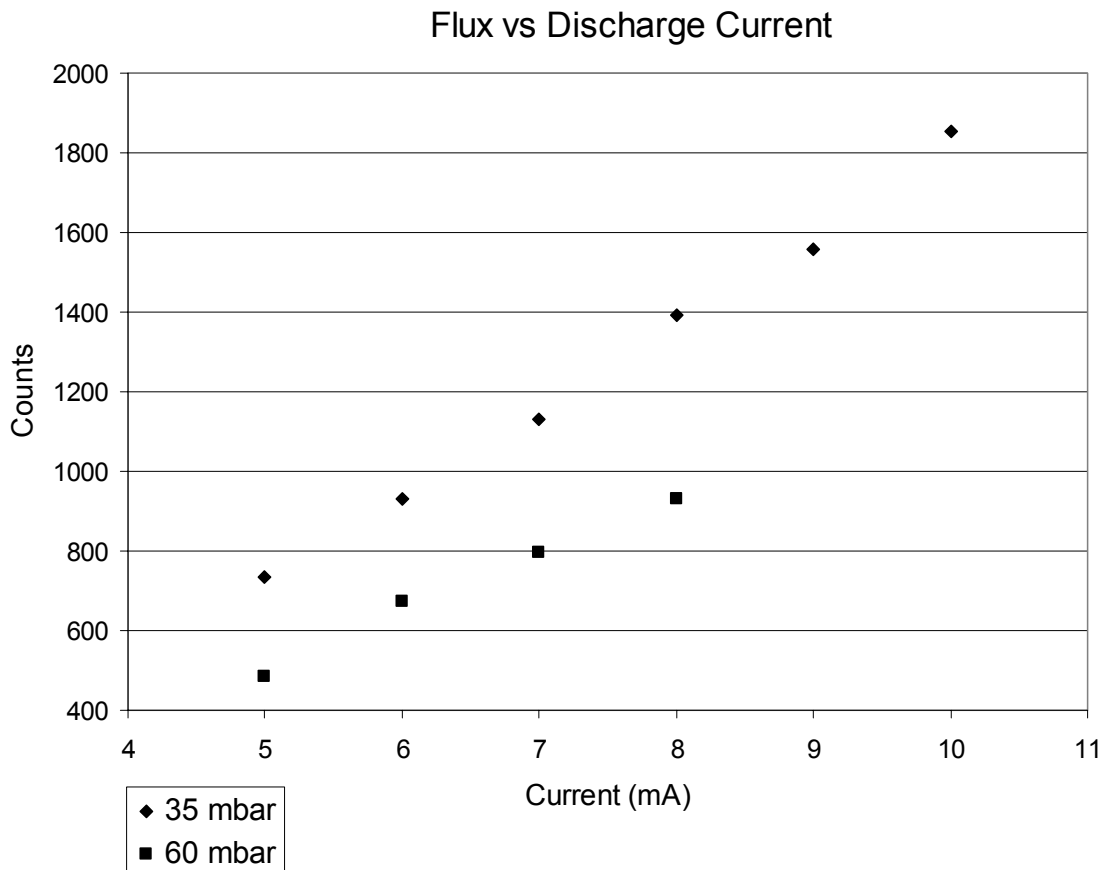


Figure 18 *Measured intensity as a function of the discharge current*

As expected the metastable helium beam intensity increases as the discharge current increases. This is simply due to the fact that at larger currents there are more electrons, which translates to a greater chance of the ground state helium atoms to be excited to metastable states. The intensity increases approximately linearly with increasing discharge current. Unfortunately there is a corresponding heating effect which leads to larger velocities.

In a separate experiment the intensity of metastable helium atoms in the beam, as a function of discharge voltage, was measured by the electron emission method (Figure 19). The driving pressure was 65 mbar. As expected the intensity increases with increasing electrode voltage.

Flux vs. Discharge Voltage

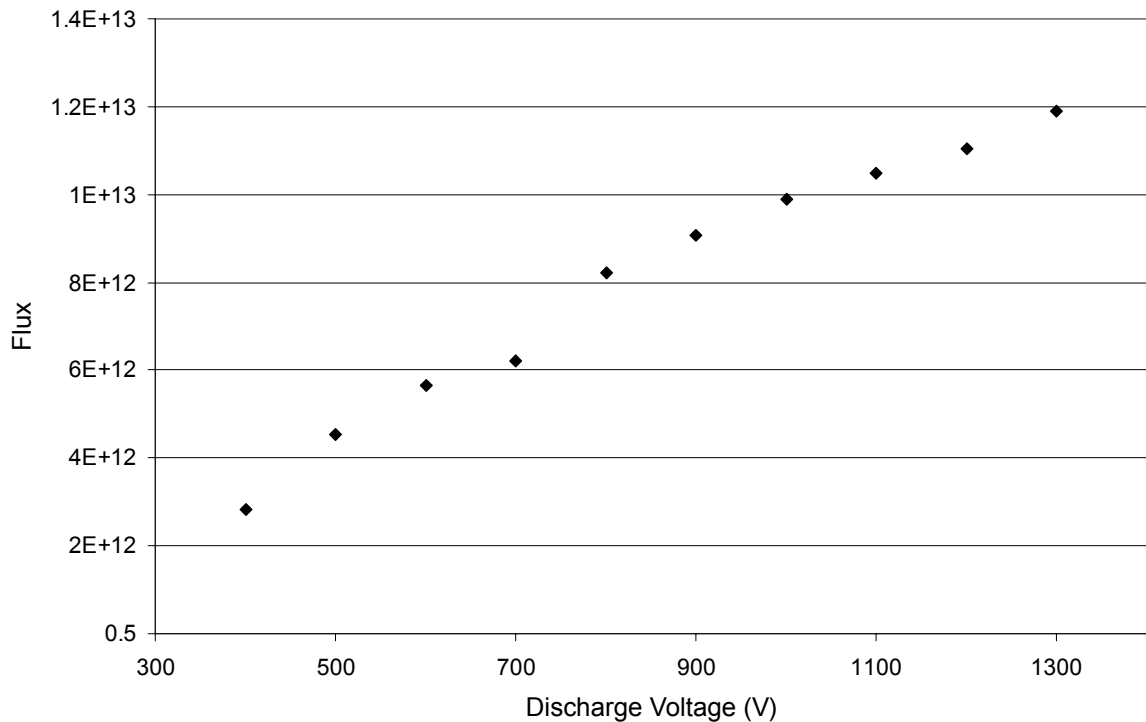


Figure 19 *Metastable flux as a function of discharge voltage*

5.1.2. Influence of Driving Pressure on He* Yield

The effect of the driving pressure on the metastable helium flux was investigated. The driving pressure inside the source was changed by using the needle valve between the helium cylinder and the helium inlet of the source.

Figure 20 shows such a measurement for a discharge current of 6 mA and a pressure in the source chamber of $3 \cdot 10^{-4}$ Torr. This pressure is fairly high when compared to other measurements since at the time the experiment was done, only a diffusion pump was connected to the source chamber. It was only later that a turbo pump was added to that chamber. As a consequence the intensity of the He* beam is slightly lower than later measurements since many of the metastable atoms are lost through collisional processes as they travel towards the skimmer.

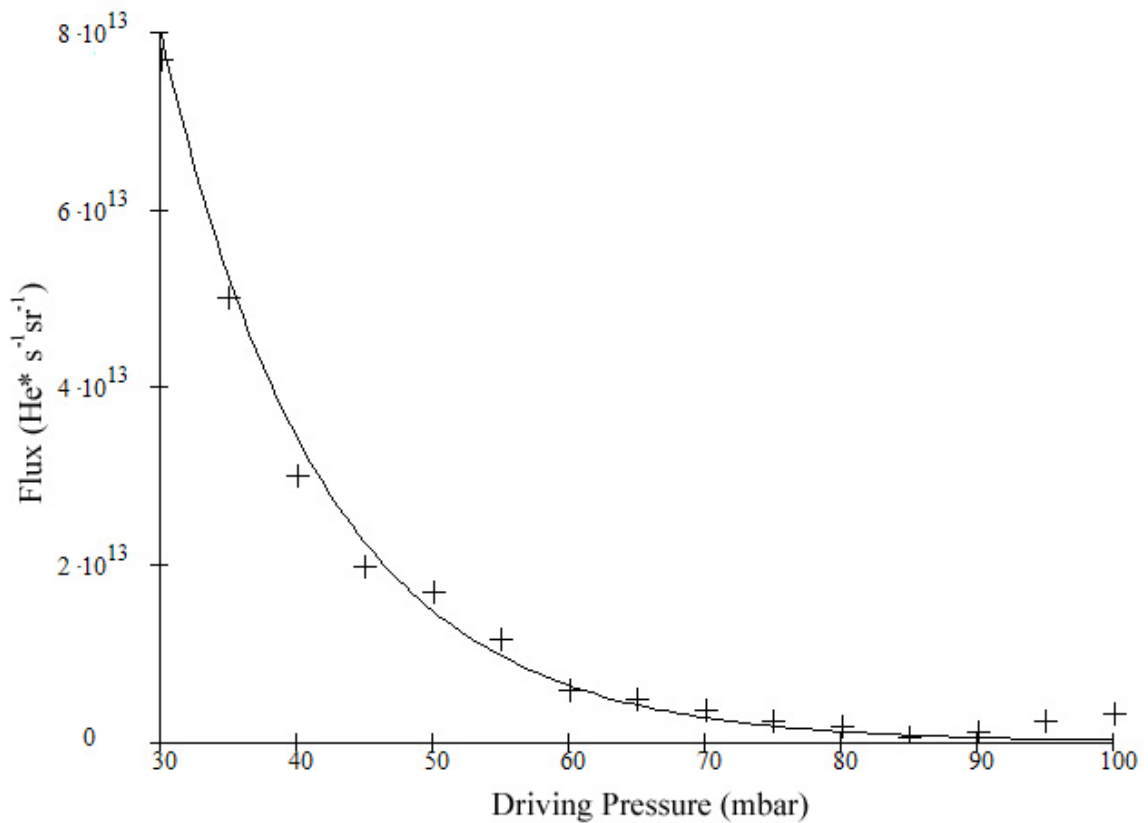


Figure 20 *Intensity of He* beam as a function of driving pressure using the electron emission method*
An explanation of the fitted exponential curve is given in section 5.1.3

It can be seen that the intensity of the metastable atoms in the beam is decreasing with increasing driving pressure and seems to tend to a minimum number at high pressures in the source. The cathode for this measurement was at 1000V, while the anode was at 200V. As the driving pressure increases, the pressure in the source chamber also increases. This leads to a higher probability of collisions between the He* atoms and the background gas, which reduces the yield of metastable atoms in the beam. At driving pressures below about 20 mbar the discharge can no longer be maintained. Future development might involve incorporating a coaxial magnetic field to contain the electrons, thereby extending the conditions for sustainable discharge to lower pressures and hopefully increasing the metastable yield.

At a discharge current of 6 mA, a driving pressure of 30 mbar and a nozzle diameter of 0.15 mm and taking into account the efficiency of the detector and the 2¹S components in the beam, the maximum He* flux was measured to be 8 · 10¹³ atoms · s⁻¹ · sr⁻¹. When the turbo pump was added this increased to 10¹⁴ atoms · s⁻¹ · sr⁻¹. By further increasing the

pumping speed (for the next generation source a 2000 l·s⁻¹ pump will be used) it is likely that the yield will be greater than 10¹⁵ atoms·s⁻¹·sr⁻¹.

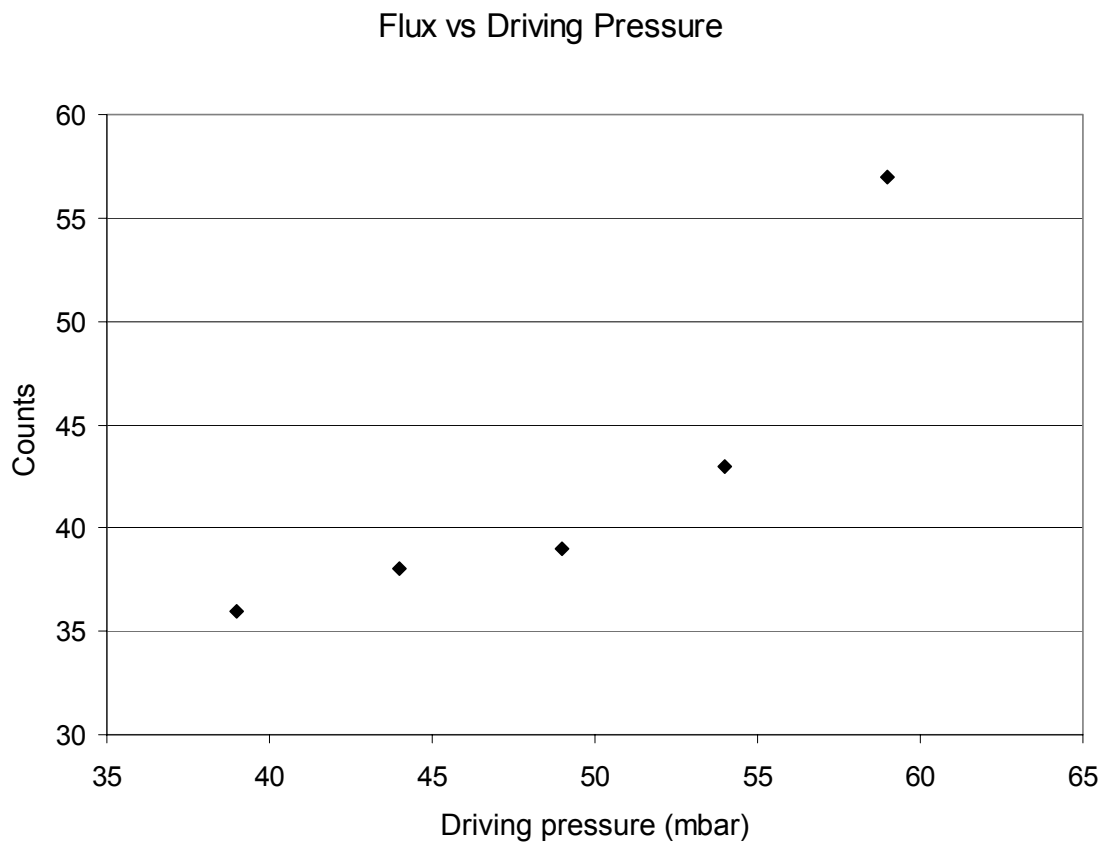


Figure 21 *He^{*} flux as a function of driving pressure with pressure in the source chamber held constant*

The above figure shows the measured beam flux as a function of the driving pressure inside the source. In this case the pressure in the surrounding source chamber was maintained at a constant pressure during the measurements, by adjusting the valve to the diffusion pump for each driving pressure. This experiment was done in an attempt to isolate the effect of the source chamber pressure.

The reason for the contrasting behaviour in Figure 20 and Figure 21 is that ambient gas in the source chamber has a detrimental effect on the metastable atoms. Calculations of this effect are given in the next section.

5.1.3. Attenuation of the Beam by Impurities

Metastable atoms can be lost from the beam by collision with impurities (Penning ionisation), and to a lesser extent by collision with other metastables and neutrals. The composition of impurities in the source chamber was measured using a residual gas analyser (Figure 22). The partial pressure of N_2 in the source chamber is quite high (was typically $2 \cdot 10^{-6}$ mbar) due to the fact that the source is in parts made of nylon, and could not be baked.

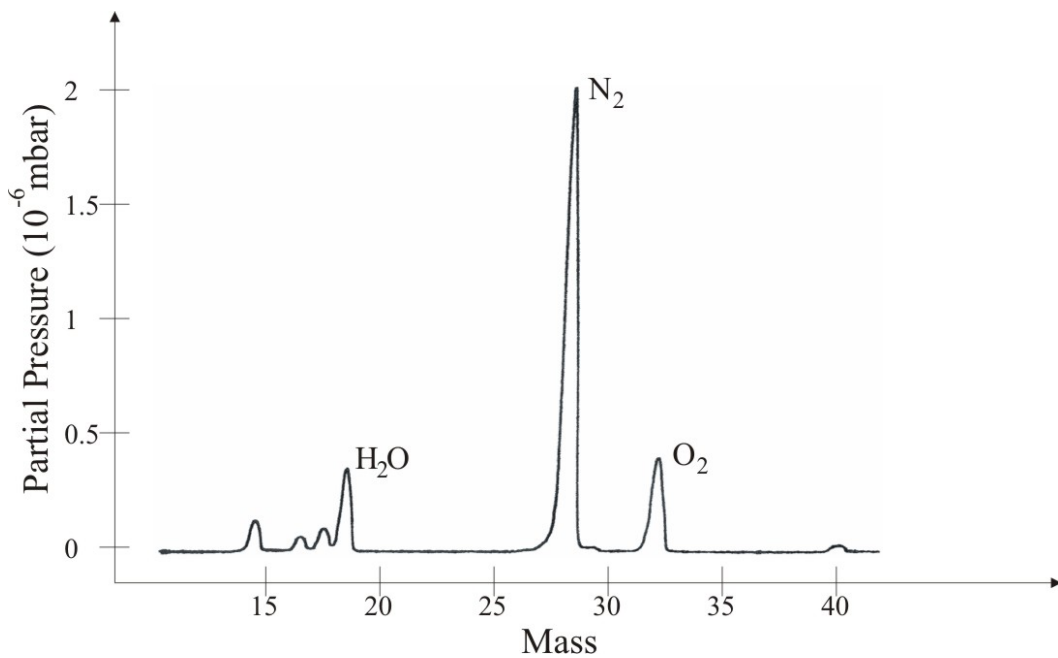


Figure 22 Residual gas spectrum from the source chamber

The intensity loss due to background gases can be calculated using Beer's law,

$$I = I_0 e^{-x/\lambda} \quad (28)$$

where x is the distance travelled through the background gas (from the nozzle to the skimmer – $x=0.05\text{m}$) and λ is the mean free path of the metastable atoms. λ depends on both the number density N of the background gas and the collision cross-section Q according to:

$$\lambda = \frac{1}{NQ} \quad (29)$$

The number density N of the background gas can be calculated using the equation $p=NkT$ (p being the partial pressure). The Penning cross-section Q is taken from reference [58] and is $Q=10^{-15}$ cm² for He(2³S) - N₂.

The exponential fit in Figure 20 gives a mean free path of metastable atoms of $\lambda = 0.83$ m. For a temperature of $T = 300$ K this corresponds to a calculated partial pressure of the impurities in the source chamber of $p = 5 \cdot 10^{-4}$ mbar. The apparent discrepancy between this value and the value measured by the residual gas analyser is most likely due to higher levels of impurities in the beam itself, coming from the discharge region.

The main conclusion from this is that a minimal distance between nozzle and skimmer in addition to the use of a high throughput pump is critical to obtain a high yield of He* atoms.

5.1.4. Influence of Source Geometry on He* Yield

The effect of the distance between the cathode and the anode on the metastable flux was investigated. It was possible to change the cathode length from the outside while the system was still under vacuum, since the cathode was sealed by an O-ring and accessible from the outside.

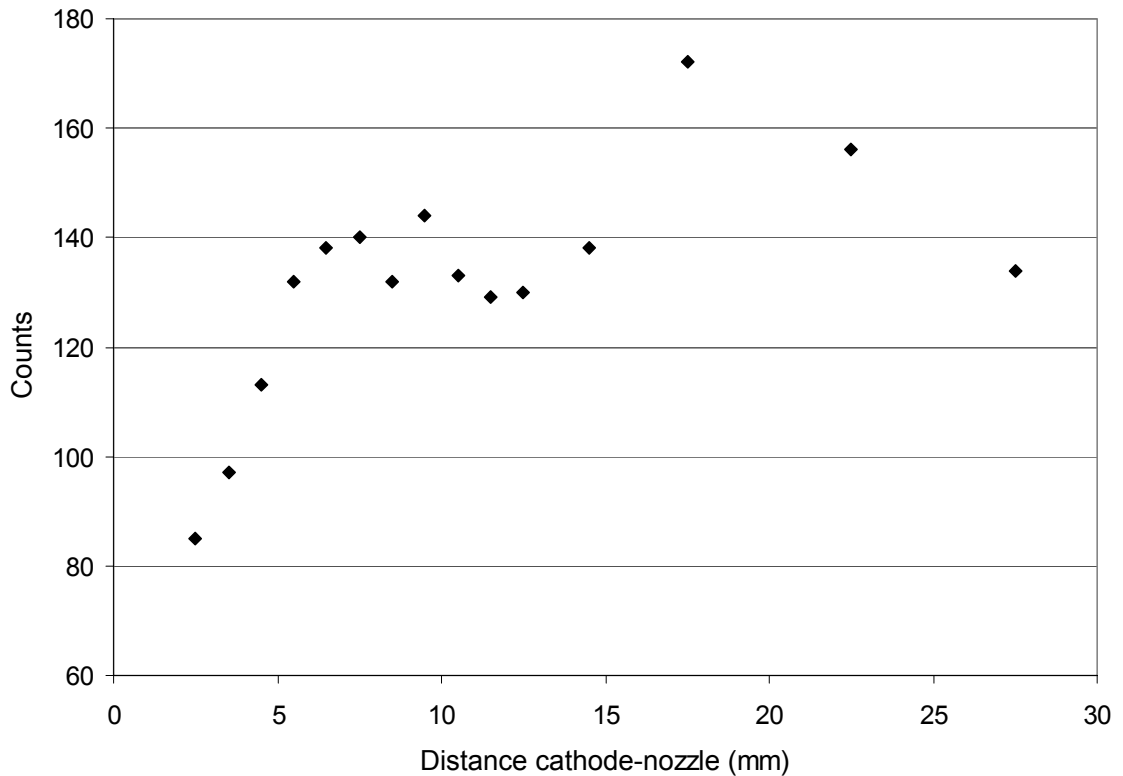


Figure 23 He^* flux as a function of cathode-nozzle distance

The general trend of the flux is to increase with cathode-nozzle distance until 17 mm and then to decrease again. The measurements should however be considered with care as the cathode might not always have been perfectly centred as it was moved, which would explain the high fluctuations with changing distance. One possible explanation is that as the distance between the cathode and the nozzle, and hence between cathode and anode increases, the electrons gain more energy as they are accelerated towards the anode and their number density increases due to ionisation. Therefore the probability of electrons exciting atoms to metastable states increases and the He^* flux increases. However, as the electrons gain more and more energy it comes to a point in the discharge where energy of the electrons is much higher than the maximum excitation cross section of the atoms and therefore they will not excite the atoms any longer [61].

The other geometric parameters that could be varied were the nozzle aperture size and the diameter of the pyrex tube surrounding the discharge. The effect of changing the aperture size is connected to the driving pressure and source chamber pressure, ie the maximum yield does not vary much but the larger the aperture is, the smaller is the

optimum driving pressure. There was some inconclusive evidence for higher yields when the discharge was confined with a smaller pyrex tube. This might be researched further, because if true, it would be useful for miniaturising the source.

5.2. Velocity Distribution

5.2.1. Longitudinal Velocity

The velocity distribution was measured by the TOF technique as described in Chapter 4.4.3. The average flow velocity is then determined by subtracting the time at which the maximum of the photon peak is recorded from the time at which the maximum of the metastable helium distribution is recorded. The distance between the chopper wheel and the channeltron divided by the time between the two maxima then gives the average flow velocity.

Figure 24 shows the measured average flow velocity of the metastable helium beam as a function of the discharge current at a driving pressure of 20 mbar in the source, a pressure in the surrounding chamber of $6 \cdot 10^{-5}$ Torr and an nozzle diameter of 0.35mm .

Velocity vs Discharge Current

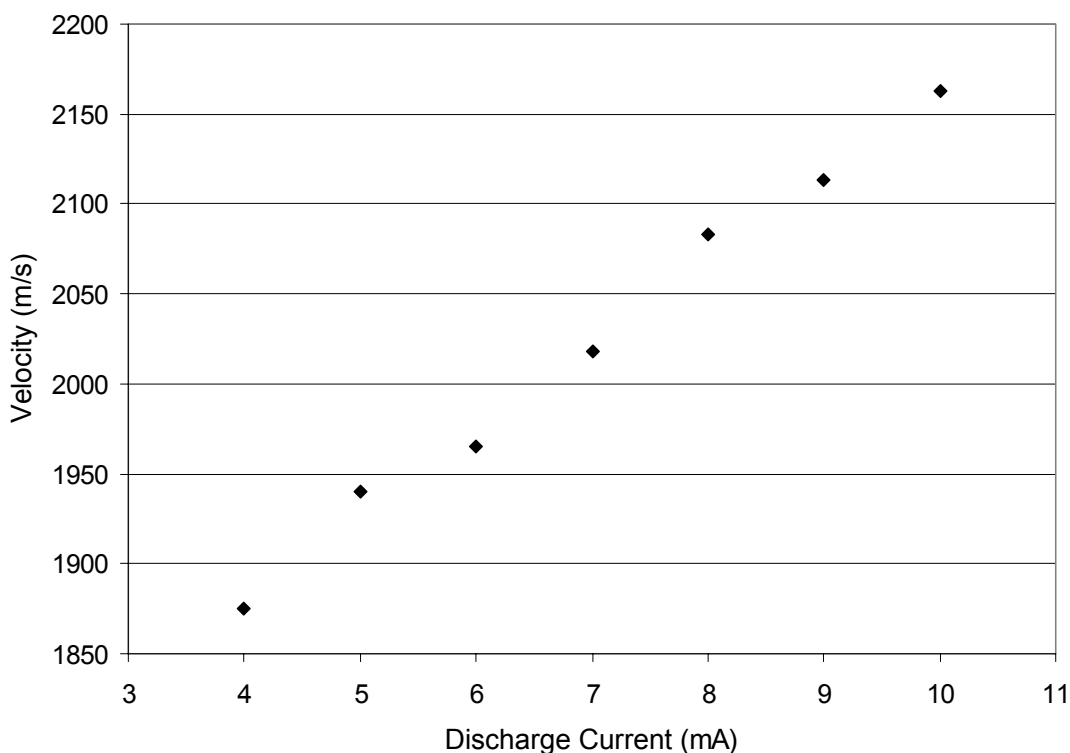


Figure 24 *Average flow velocity of He^* atoms as a function of discharge current*

An increasing discharge current means that more heat is generated in the discharge and therefore the metastable helium atoms gain more kinetic energy as they leave the source. The average velocity therefore increases with increasing discharge current.

Changing the discharge current had the effect of also changing the driving pressure. This was probably due to the fact that the ions were more attracted to the cathode, hence creating a backflow of ions and reducing the number of ions leaving the source. This increase in driving pressure with increasing discharge current could be compensated by slightly closing the needle valve to the helium cylinder, thus reducing the inflow of helium into the source.

The effect of the pressure in the source chamber on the average velocity of the He^* atoms was measured.

Velocity vs Surrounding Pressure

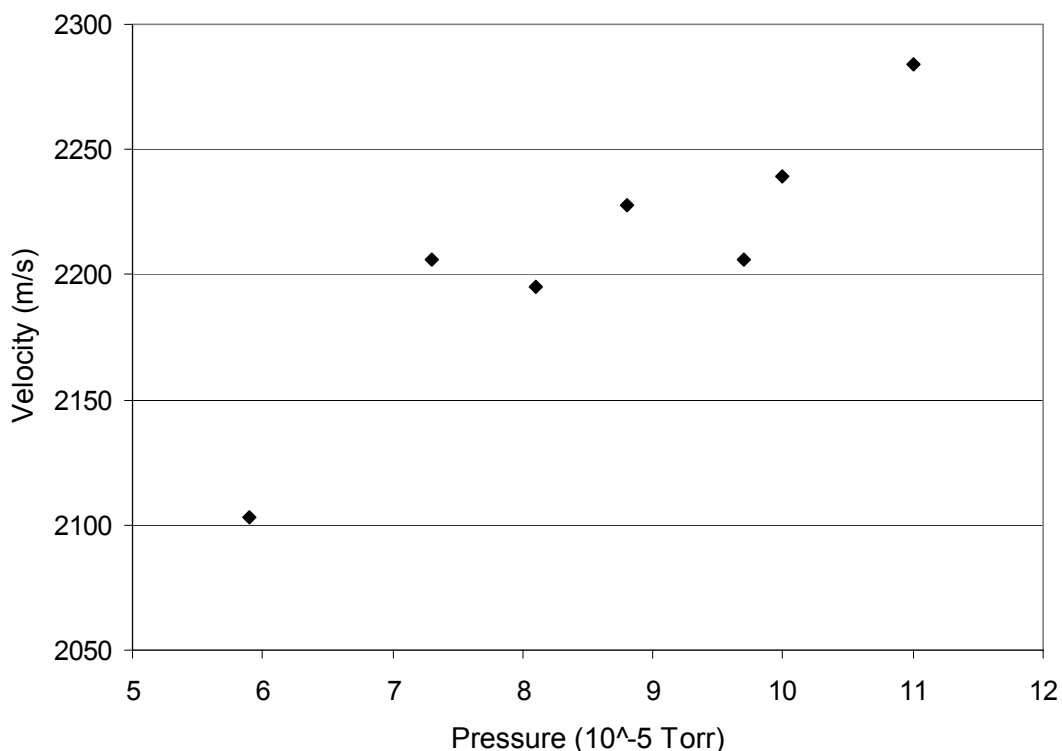


Figure 25 Average flow velocity vs pressure in the source chamber

The average flow velocity increases with increasing pressure in the source chamber, and therefore it also increases as the driving pressure rises. As the ratio of driving pressure over pressure in the source chamber increases, there is more longitudinal cooling as is indicated by equation 11, which leads to an increase in the Mach number since the velocity of sound decreases with decreasing temperature. The Mach number in our source is typically of the order of 2 as given by equation 14.

5.2.2. Velocity Width

The velocity width was measured by the TOF technique (Figure 17). The full width at half maximum (FWHM) has been calculated using Mathcad (see Appendix A4) taking into account the timing resolution of the measurement. The calculated width of the metastable distribution ΔHe^* is given by

$$\Delta He^* = \sqrt{\Delta data^2 - \Delta photon^2} \quad (30)$$

where $\Delta data$ is the measured full width at half maximum of the metastable distribution and $\Delta photon$ is the FWHM of the photon peak. This, however, is only correct if the two distributions have the same shape, and in our case it is only an approximation since the metastable distribution is approximately Gaussian whereas the photon peak has a nearly triangular shape.

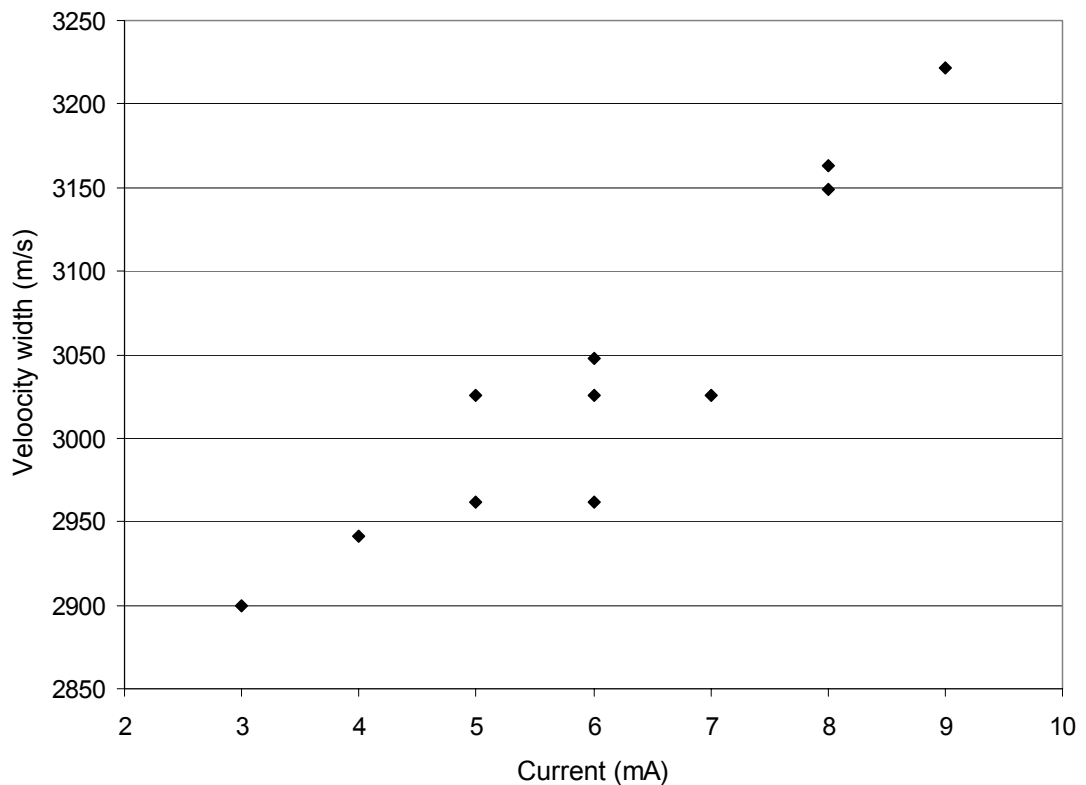


Figure 26 *Velocity width as a function of discharge current*

The velocity width increases with increasing discharge current at a constant driving pressure. This is because the Mach number decreases with discharge current since at the same pressure ratio a higher source temperature leads to a higher longitudinal temperature as indicated by equation 11. This smaller Mach number translates into a higher velocity width. Note that some measurements have been taken more than once to see the reproducibility of the measurements. The measurements were taken at around 60

mbar +/- 3 mbar with the variation in driving pressure possibly explaining the spread of data.

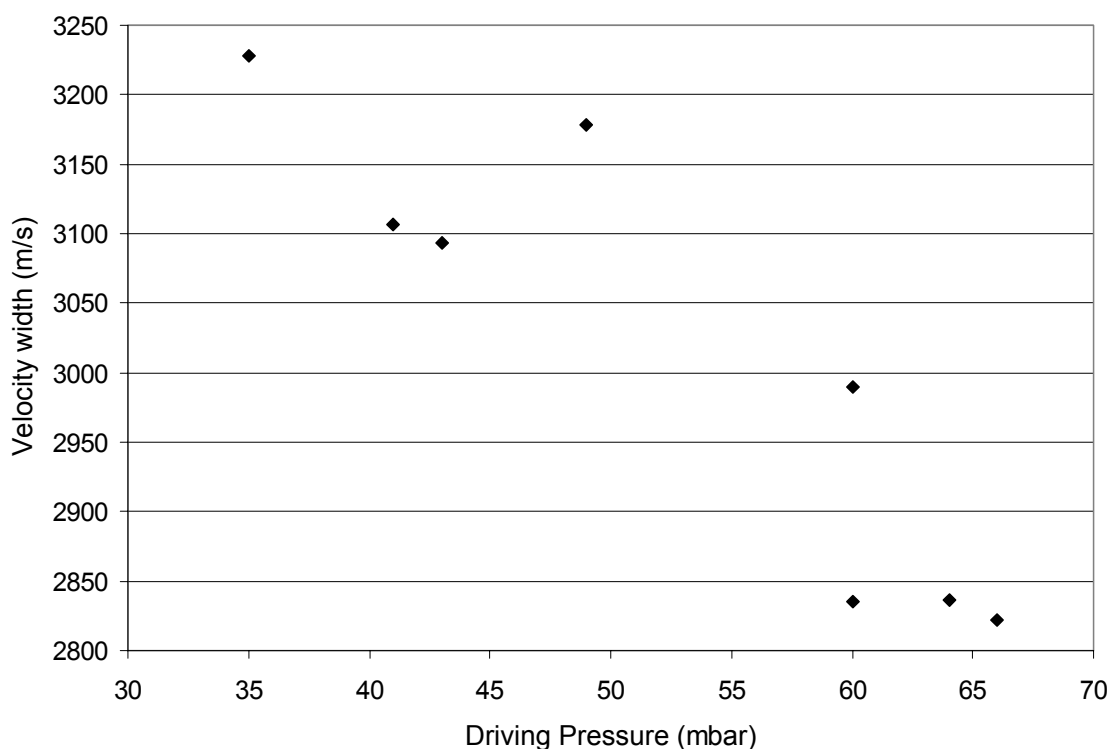


Figure 27 *FWHM of the velocity distribution of the He* beam as a function of driving pressure.*

The velocity width of the He* beam decreases with increasing driving pressure. This is because the Mach number increases with increasing driving pressure as the ratio of the source pressure to the pressure in the source chamber is higher, and therefore, as indicated by equation 11, there is more longitudinal cooling for the same discharge current.

5.3. Optimal Operating Parameters

5.3.1. Source Design Leading to Highest Yield

It was found that the highest flux was achieved using a stainless steel tube placed right in front of the nozzle of the source, rather than using a ring anode placed a few

millimetres downstream of the nozzle. Using such a tube anode also made it easier to strike a discharge. The effect of having the cathode inside a smaller pyrex tube also seemed to increase the flux.

5.3.2. Discharge Current

A low current will lead to beam with a low average velocity and a narrow velocity distribution, however at the expense of He^* flux. The velocity needs to be small so that the force on the atoms by the laser is maximised.

5.3.3. Driving Pressure

The rise in pressure in the analysis chamber was found to have no measurable effect on the flux. However, the pressure in the source chamber has a considerable effect on the flux of metastable helium atoms. The source should therefore be placed as close as possible to the skimmer, but such that there is no discharge between the anode and the cathode. The anode can alternatively be grounded to achieve that. The retarding grid in front of the source, which removes most of the electrons from the beam, needs to be at a slightly higher voltage than the anode, and an optimal voltage was at approximately 40V above the anode potential. Reducing the driving pressure will lead to an increase in He^* flux but also an increase in velocity width, which is undesirable for laser cooling.

5.4. Summary

The He^* increases with discharge current since there are more electrons in the discharge at larger current, which increases the probability of the atoms to be excited to metastable states.

The He^* intensity decreases with increasing driving pressure, since it leads to an increase in the pressure in the source chamber, which in turn increases the probability of de-excitation via collision. The effect of increasing driving pressure, while keeping the

source chamber pressure constant was also measured and it was found that the flux increased with increasing driving pressure in this case. But the effect of the increase of pressure in the source chamber is dominant.

The average velocity of the metastable atoms increases with both discharge current and driving pressure since the temperature increases with increasing current. The velocity width increases with discharge current since once again the increase in current leads to an increase in temperature. However, the velocity width decreases with increasing driving pressure since the Mach number increases with increasing driving pressure.

The cathode distance also influenced the beam quality. The flux was increased as the distance between cathode and nozzle until a point where it decreased again. The optimal distance was found to be 17mm.

Chapter 6

Conclusions and Future Work

The DC discharge as a metastable helium source is a complex environment. The flux of He^* and the velocity distribution both depend on the geometry and operating conditions in a sometimes competing fashion. The highest obtained flux in this work is 10^{14} atoms $\text{s}^{-1}\text{sr}^{-1}$, which is comparable to others in the literature. More importantly, the detailed study of the most important variables will help in future designs.

When designing the next generation source the following guidelines should be considered:

To have the highest possible metastable yield, the source should operate at a low driving pressure of no more than 30 to 40 mbar so that the pressure in the source chamber is kept low. The distance between the nozzle and the skimmer should also be small in order to reduce the probability of collisions between metastable atoms and background gas particles. An increasing current also leads to an increase in flux, however with an increase in velocity. The velocity, however, should be small so that by laser cooling the beam, as many He^* atoms as possible can be collimated.

The nozzle also plays an important role. The bigger the nozzle diameter the higher the pressure in the source chamber will be. A bigger nozzle, however, makes it easier to strike the discharge and allows for lower sustainable driving pressures. The discharge was easiest to strike when the cathode to nozzle distance was greater than 10mm. Also, the increase in cathode-nozzle distance led to an increase in He^* flux at first, but then the flux decreased again as the cathode was placed even further away from the anode. The optimal cathode-nozzle distance was approximately 17 mm. The shape of the anode was also critical. A stainless steel tubular anode placed just behind the nozzle on the low

pressure side was found to produce an increase in flux by a factor of 20 when compared to a ring anode placed a few millimetres downstream of the anode. In addition, while with the ring anode setup a discharge could only be maintained at very high voltages, the tubular anode provided discharges at much lower voltages.

In future experiments a cathode array could be used to increase the yield of metastable atoms. The interaction between the different shock fronts from the different ‘microsources’ must be investigated to see the interaction between them. The interaction between two parallel supersonic jets has been modelled by Gidalevich *et al.* [62]. Magnetic mirrors might also be used to create a plasma downstream of the anode. In this plasma, electrons and ions will be constraint and collisions will occur more frequently. Eventually they will reach the loss cone from where they can escape the plasma. Since the electrons in this region bounce back and forth between the magnetic mirrors, the probability of them to excite an atom to the metastable state will be increased.

The source should also be cooled with liquid nitrogen or even liquid helium in order to decrease the average flow velocity of the He* atoms and to narrow the velocity distribution. The most crucial part of the source that needs cooling is the nozzle, since this is where the metastable atoms are expanding into the low pressure region.

It is expected that, with these considerations taken into account the next generation source will have a metastable flux exceeding 10^{15} atoms $s^{-1}sr^{-1}$. With liquid nitrogen cooling, the average velocity will be less than 1000 $m s^{-1}$ and a velocity width corresponding to a Mach number of greater than 2.

Appendix

A1. MCS software

The software used to acquire the TOF spectra was the MCS-32 provided by Perkin-Elmer.

The pass length, the dwell time and the total number of passes can be set under the menu *Acquire – Pass Control*.

The pass length gives the number of bins the multichannel scaler (MCS) fills up before it waits for a trigger to begin with the next sweep. Each pass the MCS adds the counts to the previous ones. If an external trigger is selected, as is the case in this work, the MCS-32 software will only begin a new sweep if a triggering signal is registered after the pass length has expired. The pass length must be set so that long enough for the whole spectrum (ie photon + metastable distribution) to be recorded, but short enough for it to trigger each time the slit passes through the beam line. The chopper wheel used in this work had a slit as well as a hole, so that it would trigger very shortly before the slit passes the beam line. The pass length must therefore be set such that it does not trigger twice in one revolution, ie long enough so that it would trigger when the hole passes the electro-optical switch, but short enough that the slit passes the trigger during that pass length so that the software would not register the triggering signal. The optimal pass length was found to be 7000 with a dwell time of 1 μ s.

The dwell time gives the time the MCS-32 software waits before it advances to the next bin. During this time it adds up all the counts in the same channel. The pass length times the dwell time gives the time each pass lasts.

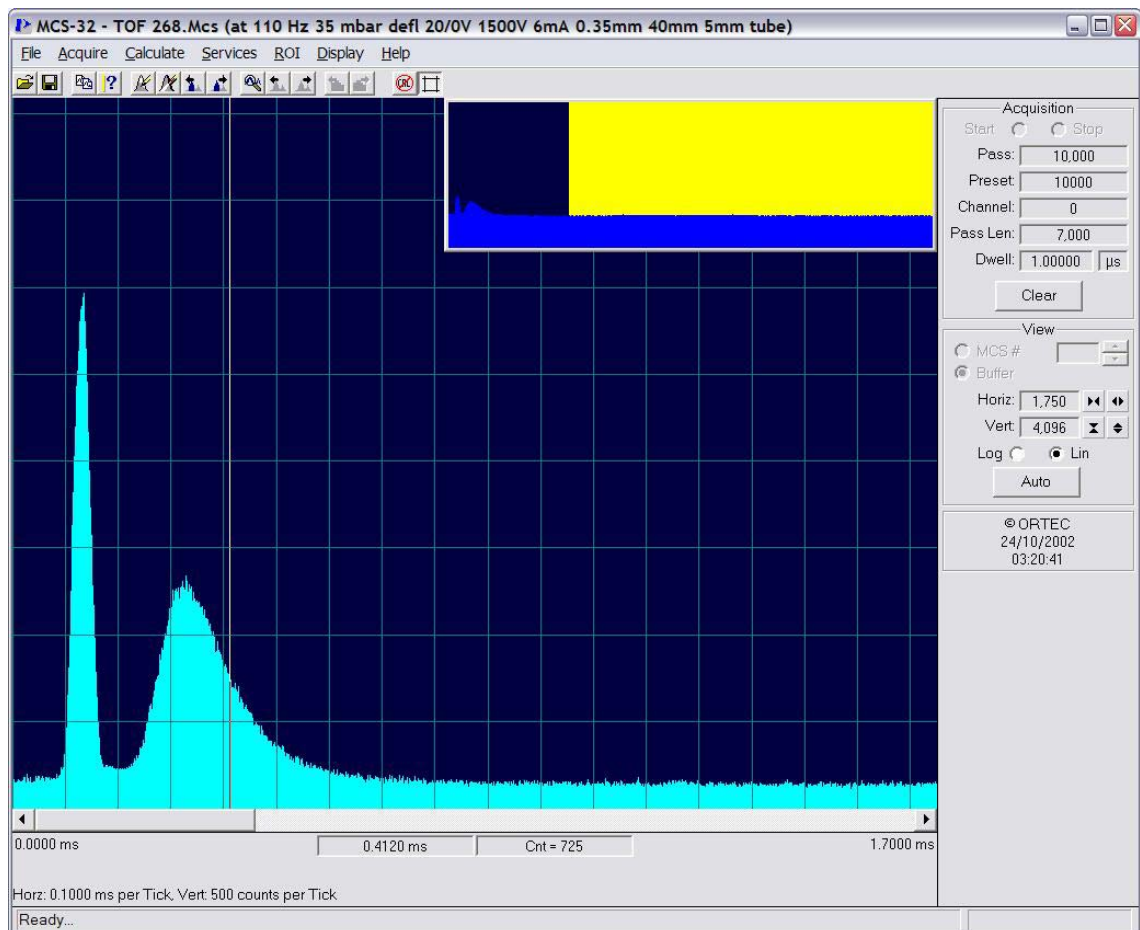


Figure 28 *MCS-32 software for the TOF measurements*

The amplified signal from the channeltron is fed into the “IN” input on the MCS card. This is the BNC connector on the rear panel of the card and accepts analogue or digital pulses of up to $\pm 5V$ in amplitude. The pulses are counted as they cross the discriminator threshold.

A2. Setup of Pre-amp for TOF measurements

In order to measure the pulses with the MCS-PCI card in the PC, the signal first needs to be amplified. The threshold of the Pre-amp must also be set such as to minimise the background noise.

The pre-amp used in this experiment was the Amptek A-101, which initially has a nominal threshold of $1.6 \cdot 10^{-13}$ Coulombs. This is equivalent to 10^6 electrons per pulse.

The threshold can be increased by the addition of a resistor between pin 9 and 12, R_t in parallel with the 10 k Ω resistor. Thus as R_t decreases, the threshold increases.

A variable resistor of 0 to 5 kV was put in parallel with the 10 k Ω resistor. The optimal threshold was found to be with a total resistance $R_t = 180$ k Ω .

A3. Trigger for MCS

The trigger used for the multichannel scaler was an opto-switch from Honeywell (part: HOA6990-T51), which is a Schmitt trigger delivering a TTL signal of 5 V each time the hole in the chopper wheel passes through the gap of the opto-switch.

The connections to the leads of the trigger are given in the following table.

Lead colour	Red	Black	Green	White	Blue
Meaning	Anode	Cathode	Ground	V_{cc}	V_{out}
Voltage	0.66 V	0 V	0 V	5 V	5 V TTL

Where V_{cc} is the operating voltage of the trigger and is set to 5 V with a current of 10 mA. The Trigger anode is set to 0.66 V with a current of 15 mA.

The triggering signal is fed into the “START IN” input on the card. This input was situated on a 25 pin D-type connector on the back of the card, and hence a cable needed to be made to be able to connect a BNC cable to it.

A4. Program to analyse data in Mathcad

The maxima of the TOF spectrum can be found by using the following function

$$\text{Max}(D) := \left| \begin{array}{l} j \leftarrow 0 \\ \text{for } i \in 100..900 \\ \quad \text{if } D_i > D_{i-100} \text{ if } D_i > D_{i+100} \text{ if } D_i > D_{i+1} \text{ if } D_{i-1} < D_i \\ \quad \quad \left| \begin{array}{l} \text{max}j \leftarrow i \\ j \leftarrow j + 1 \end{array} \right. \\ \text{max} \end{array} \right.$$

The TOF spectrum is then smoothed before analysing it

$$\text{smooth}(D) := \text{ksmooth}(D^{(0)}, D^{(1)}, 0.020)$$

The TOF of the He* atoms is then given by the difference of the two maxima

$$\text{TOF}(D) := \text{Max}(\text{smooth}(D))_1 - \text{Max}(\text{smooth}(D))_0$$

The velocity is given by the distance between chopper wheel and channeltron over the T

$$\text{Dist} := 0.45$$

$$\text{Velocity}(D) := \frac{\text{Dist}}{\text{TOF}(D) \cdot 10^{-6}} \quad \text{Intensity}(D) := \text{smooth}(D)_{\text{Max}(\text{smooth}(D))_1}$$

$$\text{Max}(\text{smooth}(s(\text{TOF266}))) = \begin{pmatrix} 139 \\ 339 \end{pmatrix}$$

$$\text{Velocity}(s(\text{TOF266})) = 2.25 \times 10^3$$

$$\text{Intensity}(s(\text{TOF266})) = 1.316 \times 10^3$$

To identify the two peaks, the minimum between them must be worked out

$$\text{Min}(D) := \left| \begin{array}{l} \text{for } i \in 100.. \text{rows}(D) - 101 \\ \quad \text{min} \leftarrow i \text{ if } D_{i+100} > D_i \text{ if } D_{i-100} > D_i \text{ if } D_{i+1} > D_i \text{ if } D_{i-1} > D_i \\ \text{min} \end{array} \right.$$

$$\text{Min}(\text{smooth}(s(\text{TOF266}))) = 216$$

The width at half maximum of the two peaks is then given by the functi

```

Res(data) := | j ← 0
              | res0 ← 0
              | res1 ← 0
              | max ← Max(data)
              | break if rows(max) > 2
              | for i ∈ 0..Min(data)
              |   res0 ← res0 + 1 if datai >  $\frac{\text{data}_{(\text{max}_0)}}{2}$ 
              | for i ∈ Min(data)..rows(data) - 1
              |   res1 ← res1 + 1 if datai >  $\frac{\text{data}_{(\text{max}_1)}}{2}$ 
              | res

```

$$\text{Res}(\text{smooth}(s(\text{TOF266}))) = \begin{pmatrix} 43 \\ 159 \end{pmatrix}$$

Which gives a FWHM of:

$$\text{FWHM}(\text{data}) := \frac{\text{Dist}}{\sqrt{(\text{Res}(\text{data})_1)^2 - (\text{Res}(\text{data})_0)^2} \cdot 10^{-6}}$$

$$\text{FWHM}(\text{smooth}(s(\text{TOF266}))) = 2.94 \times 10^3$$

The TOF spectrum needed to be smoothed to be able to analyse it. This was also done in mathcad, and the function used to smooth the signal used a Gaussian kernel to compute the local weighted averages of the data. Figure 29 shows an example of a smoothed function compared to the original function.

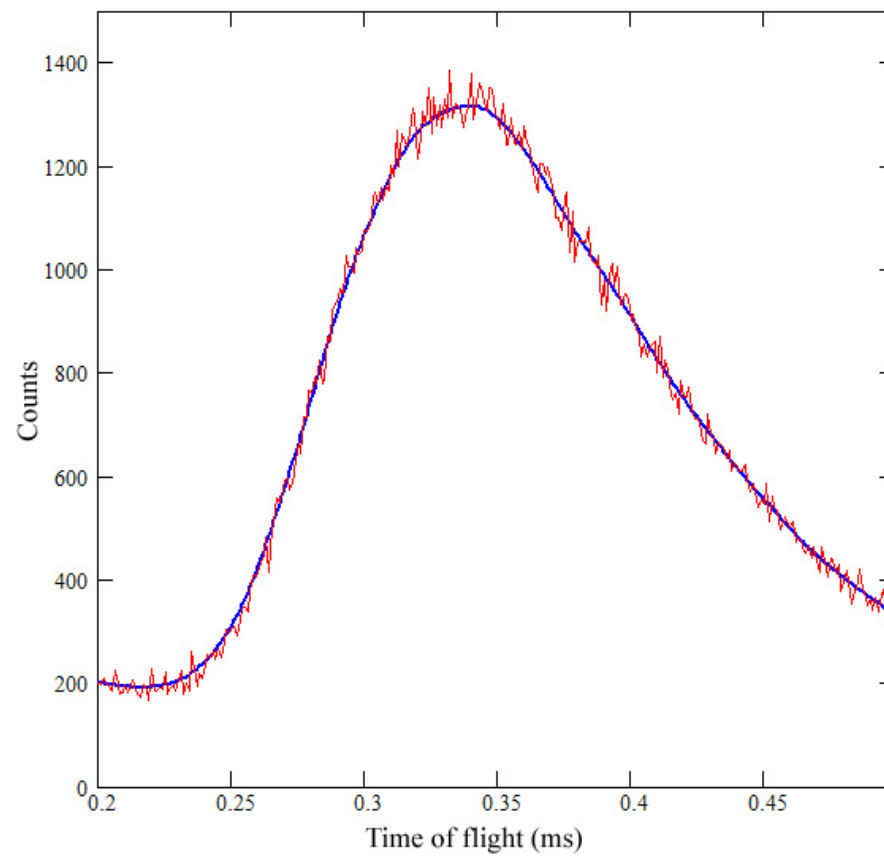


Figure 29 *Smoothed spectrum compared to original spectrum*

References

- [1] H Conrad, G Ertl, J Küppers, W Sesselmann and H Haberland, *Surf. Sci.* **100** (1980) L461
- [2] L G Christophorou (ed) *Electron Molecule Interactions* vols 1 and 2 (1984) Orlando, FL: Academic
- [3] E W Rothe, R H Neynaber, S M Trujillo, *J. Chem. Phys.* **42** (1965) 3310
- [4] G W F Drake, *Phys. Rev. A* **3** (1971) 908
- [5] J R Woodworth and H Warren Moos, *Phys. Rev. A* **12** (1975) 2455
- [6] D W Fahey, W F Parks and L D Schearer, *J. Phys. E: Sci. Instrum.* **13** (1980) 381
- [7] M J Verheijen, H C W Beijerinck, L H A M v. Moll, J Driessen and N F Verster *J. Phys. E* **17** (1984) 904
- [8] W L Borst, *Physical Review A* **9** (1974) 1195
- [9] B Brutschy and H Haberland, *J. Phys. E: Sci. Instrum.* **10** (1977) 90
- [10] Y Yamauchi, M Kurahashi and N Kishimoto, *Meas. Sci. Technol.* **9** (1998) 531
- [11] M Kurahashi and Y Yamauchi, *Nucl. Instr. and Meth. in Phys. Res. B* **173** (2001) 516
- [12] R Weis, C Winkler and R W Schrittwieser, *Plasma Sources Sci. Technol.* **6** (1997) 247
- [13] W Rooijackers, W Hogervorst and W Vassen, *Opt. Commun.* **123** (1996) 321
- [14] G R Woestenenk, J W Thomsen, M van Rijnbach, P van der Straten and A Niehaus, *Rev. Sci. Instrum.* **72** (2001) 3842
- [15] T W Riddle, M Onellion, F B Dunning and G K Walters, *Rev. Sci. Instrum.* **52** (1981) 797
- [16] R D Rundel, F B Dunning and R F Stebbings, *Rev. Sci. Instrum.* **45** (1974) 116
- [17] P D Johnson and T A Delchar, *J. Phys. E: Sci. Instrum.* **10** (1977) 428
- [18] T Halfmann, J Koensgen and K Bergmann, *Meas. Sci. Technol.* **11** (2000) 1510
- [19] P G A Theuws, H C W Beijerinck, N F Verster and D C Schram, *J. Phys. E: Sci. Instrum.* **15** (1982) 573
- [20] J Q Searcy, *Rev. Sci. Instrum.* **45** (1974) 589
- [21] E L Leasure, C R Müller and T Y Ridley, *Rev. Sci. Instrum.* **46** (1975) 635
- [22] I I Fabrikant, O B Shpenik, A V Snegursky, A N Zavilolpulo, *Phys. Repts.* **159** (1988) 1

-
- [23] J P Simons, K Suzuki and C Washington, *J. Phys. E: Sci. Instrum.* **17** (1984) 581
- [24] T A Delchar and D A MacLennan, *J. Chem. Phys.* **50** (1969) 1179
- [25] A S Bell, B Brezger, U Drodofsky, S Nowak, T Pfau, J Stuhler, Th Schulze and J Mlynek, *Surf. Sci.* **435** (1999) 40
- [26] A S Bell, T Pfau, U Drodofsky, J Stuhler, Th Schulze, B Brezger, S Nowak and J Mlynek, *Microelect. Eng.* **42** (1998) 587
- [27] S Nowak, T Pfau and J Mlynek, *Microelect. Eng.* **35** (1997) 427
- [28] F Pereira Dos Santos, J Leonard, Junmin Wang, C J Barrelet, F Perales, E Rasel, C S Unnikrishnan, M Leduc and C Cohen-Tannoudji, *Phys. Rev. Lett.* **86** (2001) 3459
- [29] W Vassen, *At. Opt. Interfer.* **2** (2001) 613
- [30] H D Hagstrum, *Phys. Rev.* **96** (1954) 336
- [31] Y Harada, S Masuda and H Ozaki, *Chem. Rev.* **97** (1997) 1897
- [32] H D Hagstrum, *Phys. Rev. Lett.* **43** (1979) 1050
- [33] N Lorente, M A Cazalilla, J-P Gauyacq, D Teillet-Billy and P M Echenique, *Surf. Sci.* **411** (1998) L888
- [34] F Bozso, J T Yates, J Arias, H Metiu and R M Martin, *J. Chem. Phys.* **78** (1983) 4256
- [35] H Conrad, G Ertl, J Küppers, S W Wang, K Gérard and H Haberland, *Phys. Rev. Lett.* **42** (1979) 1082
- [36] Y Harada, *Surf. Sci.* **158** (1985) 455
- [37] D M Oró, P A Soletzky, X Zhang, F B Dunning and G K Walters, *Phys. Rev.* **A49** (1994) 4703
- [38] D M Oró, Q Lin, P A Soletzky, X Zhang, F B Dunning and G K Walters, *Phys. Rev.* **B46** (1992) 9893
- [39] W Keller, H Morgner and W A Müller, *Mol. Phys.* **58** (1986) 1039
- [40] W Sesselmann, H Conrad, G Ertl, J Küppers, B Woratschek and H Haberland, *Phys. Rev. Lett.* **50** (1983) 446
- [41] M Onellion, M W Hart, F B Dunning, *Phys. Rev. Lett.* **52** (1984) 380
- [42] J J McClelland, *Handbook of Nanostructured Materials and Technology*, Academic Press, San Diego (2000)
- [43] A Bard, K K Berggren, J L Wilbur, J D Gillaspay, S L Rolston, J J McClelland, W D Phillips, M Prentiss and G M Whitesides, *J. Vac. Sci. Technol. B* **15**(5) (1997) 1805

-
- [44] S B Hill, C A Haich, F B Dunning, G K Walters, J J McClelland, R J Celotta and H G Craighead, *Appl. Phys. Lett.* **74** (1999) 2239
- [45] Y Xia, X Zhao, E Kim and G M Whitesides, *Chem. Mater.* **7** (1995) 2332
- [46] M P Seah and W A Dench, *Surf. Interface Anal.* **1** (1979) 2
- [47] J H Thywissen, K S Johnson, R Younkin, N H Dekker, K K Berggren, A P Chu, M Prentiss and S A Lee, *J. Vac. Sci. Technol. B* **15**(6) (1997) 2093
- [48] A Ashkin, *Phys. Rev. Lett.* **25** (1970) 1321
- [49] R Frisch, *Z. Phys.* **86** (1933) 42
- [50] T W Hänsch and A L Schawlow, *Opt. Comm.* **13** (1975) 68
- [51] D J Wineland and H Dehmelt, *Bull. Am. Phys. Soc.* **20** (1975) 637
- [52] H J Metcalf, P van der Straten, *Laser cooling and trapping* (1999) Springer-Verlag, New York
- [53] F B Dunning and R G Hulet (eds.), *Atomic, Molecular and Optical Physics: Atoms and Molecules*, volume **29B** (1996) Academic Press, London
- [54] N F Ramsey, *Thermal Beam Sources in Methods of Experimental Physics: Atomic, Molecular and Optical Physics*, Vol. II (1993) R Hulet and FB Dunning (eds.), Academic Press, New York
- [55] Weijian Lu, *Laser Manipulation of a Metastable Helium Beam for Atom Lithography*, PhD Thesis, Australian National University (1999)
- [56] M D Morse, *Supersonic Beam Sources in Atomic, Molecular and Optical Physics: Atoms and Molecules*, volume 29B (1996) F B Dunning and R G Hulet (eds.), Academic Press, London
- [57] A Chambers, R K Fitch, B S Halliday, *Basic Vacuum Technology, 2nd ed.* (1998) Institute of Physics Publishing
- [58] K Ohno, T Takami, K Mitsuke and T Ishida, *J. Chem. Phys.* **94** (1991) 2675
- [59] H Ferkel, R Feltgen and D Pikorz, *Rev. Sci. Instrum.* **62** (1991) 2626
- [60] F B Dunning, R D Rundel and R F Stebbings, *Rev. Sci. Instrum.* **46** (1975) 697
- [61] Y P Raizer, *Gas Discharge Physics*, (1991) Springer Verlag, Berlin
- [62] E Gidalevich, R L Boxman and S Goldsmith, *J. Phys. D: Appl. Phys.* **31** (1998) 304